Gauging a Hydrocarbon Ruler by an Intrinsic Exciton Probe[†]

M. Adil Khan,[‡,§] Chris Neale,[‖] Catherine Michaux,[⊥] Régis Pomès,[‖,@] Gilbert G. Privé,[‖,⊥] Robert W. Woody,[#] and Russell E. Bishop*,[‡,§,‖]

*Departments of Laboratory Medicine and Pathobiology and of Biochemistry, University of Toronto, Toronto,
ON, Canada M5S 1A8, Department of Medical Biophysics, University of Toronto, and Division of Molecular and
Structural Biology, Ontario Cancer Institute, Toronto, ON, Canada M5G 2M9, Department of Structural Biology and
Biochemistry, Hospital for Sick Children, Toronto, ON, Canada M5G 1X8, Department of Biochemistry and Molecular Biology,
Colorado State University, Fort Collins, Colorado 80523, and Department of Biochemistry and Biomedical Sciences,
McMaster University, Hamilton, ON, Canada L8N 3Z5*

ABSTRACT: The structural basis of lipid acyl-chain selection by membrane-intrinsic enzymes is poorly understood because most integral membrane enzymes of lipid metabolism have proven refractory to structure determination; however, robust enzymes from the outer membranes of Gram-negative bacteria are now providing a first glimpse at the underlying mechanisms. The methylene unit resolution of the phospholipid: lipid A palmitoyltransferase PagP is determined by the hydrocarbon ruler, a 16-carbon saturated acyl-chain-binding pocket buried within the transmembrane β-barrel structure. Substitution of Gly88 lining the floor of the hydrocarbon ruler with Ala or Met makes the enzyme select specifically 15- or 12-carbon saturated acyl chains, respectively, indicating that hydrocarbon ruler depth determines acyl-chain selection. However, the Gly88Cys PagP resolution does not diminish linearly because it selects both 14- and 15-carbon saturated acyl chains. We discovered that an exciton, emanating from a buried Tyr26−Trp66 phenol−indole interaction, is extinguished by a local structural perturbation arising from the proximal Gly88Cys PagP sulfhydryl group. Site-specific S-methylation of the single Cys afforded Gly88Cys-S-methyl PagP, which reasserted both the exciton and methylene unit resolution by specifically selecting 13-carbon saturated acyl chains for transfer to lipid A. Unlike the other Gly88 substitutions, the Cys sulfhydryl group recedes from the hydrocarbon ruler floor and locally perturbs the subjacent Tyr26 and Trp66 aromatic rings. The resulting hydrocarbon ruler expansion thus occurs at the exciton's expense and accommodates an extra methylene unit in the selected acyl chain. The hydrocarbon ruler−exciton juxtaposition endows PagP with a molecular gauge for probing the structural basis of lipid acyl-chain selection in a membrane-intrinsic environment.

The diversity of acyl chains found in membrane lipids reflects the ability of cells to modulate membrane biophysical states and to employ specific lipids in signal transduction pathways (*1*, *2*). Enzymes of lipid metabolism encounter an effective combinatorial library in their substrates and are necessarily endowed with mechanisms for selecting specific acyl-chain types. Most lipid-metabolizing enzymes of known structure represent soluble globular domains that exist either free in solution or as monotopic membrane proteins (*3*, *4*). Some of these structures indicate how enzymes interact with soluble lipid substrates and have revealed acyl-chain-measuring devices known as hydrocarbon rulers (*5*, *6*). The monotopic membrane enzyme structures further indicate how globular domains interact with their substrates at the periphery of lipid bilayers. However, many key lipid metabolic steps are catalyzed by integral membrane enzymes, which are embedded in their substrates and encounter a low-dielectric milieu not normally accessible to soluble globular protein domains. The biophysical basis of integral membrane lipid−protein recognition is advancing with increasing numbers of determined structures, but integral membrane enzymes of lipid metabolism have mostly proven refractory to structure determination (*7*). Exceptions are found in the outer membranes of Gram-negative bacteria, which have recently revealed integral membrane protein structures for a phospholipase, a lipid deacylase, and a lipid acyltransferase (*8−11*). These integral membrane β-barrel enzymes are more robust than most α-helical integral membrane enzymes of lipid metabolism, and are now providing insights into the molecular mechanisms of lipid acyl-chain selection within a lipid bilayer environment.

Many integral membrane β-barrel proteins can be purified in an unfolded state and refolded at high concentrations in

* To whom correspondence should be addressed: Department of Biochemistry and Biomedical Sciences, McMaster University, Hamilton, ON, Canada L8N 3Z5. Telephone: (905) 525-9140, ext. 28810. Fax: (905) 522-9033. E-mail: bishopr@mcmaster.ca.

[‡] Department of Laboratory Medicine and Pathobiology, University of Toronto.

[§] McMaster University.

[‖] Department of Biochemistry, University of Toronto.

[⊥] Department of Medical Biophysics, University of Toronto, and Ontario Cancer Institute.

[@] Hospital for Sick Children.

[#] Colorado State University.

detergent micelles, which are transparent to certain spectroscopic analyses of protein structure and stability. Extrinsic spectroscopic probes can be introduced into proteins to study structure−function relationships, but these studies must be carefully scrutinized to avoid artifacts arising from structural perturbations introduced by the probe itself. If Trp and Tyr residues are localized in a functionally interesting protein region, their aromatic side chains can be exploited as intrinsic probes to prevent such artifacts. However, it can be difficult or impossible to deconvolute the signals that arise from a single aromatic side chain if multiple copies are present in a given protein. More rarely, two or more Trp and/or Tyr residues that interact within specific geometrical and distance constraints can afford a so-called exciton interaction. The exciton effect arises from the delocalization of the excited states of two interacting chromophores (*12*). The strong $\pi \rightarrow \pi^*$ transitions arising from Trp and Tyr side chains do not on their own generate Cotton effects that can be detected by circular dichroism (CD)[1] spectroscopy. Cotton effects arise when parallel components of electric and magnetic dipole transition moments are combined, and strict group theoretical rules show that this cannot happen when a chromophore possesses centers or planes of symmetry (*13*). When they are placed in a chiral environment, such as that provided by the polypeptide backbone of a protein molecule, an exciton effect arising from a pair of interacting chromophores can generate two Cotton effects of equal magnitude and opposite sign that are slightly separated by the so-called Davydov energy (*14*). The resultant of these two overlapping Cotton effects is a bisignate curve known as an exciton couplet, which can be detected in the far-UV region of a protein CD spectrum (*15*).

Exciton theory lies at the heart of protein CD spectroscopy because it accounts for key spectroscopic signatures that arise between $\pi \rightarrow \pi^*$ transitions in interacting peptide groups located within the secondary structural elements. However, exciton couplets arising from interacting aromatic side chains have largely been ignored in protein secondary structure analysis, despite their clear overlap in the far-UV range with the signals that arise from secondary structure (*16*). Due to the strong rotational strengths associated with the α-helix, the weaker aromatic exciton couplets in the far-UV range are most apparent in proteins with low α-helical content, but their presence can significantly influence the far-UV CD spectrum of any protein (*17*, *18*). Theoretical analyses show that exciton couplets arising from aromatic side-chain interactions are among the more reliably predicted CD spectroscopic signatures that can occur within a protein molecule (*19*). Algorithms that consider aromatic exciton interactions for predicting a protein CD spectrum from a given set of crystal structure coordinates are available. One can usually pinpoint interacting aromatic side chains associated with an exciton couplet by systematically replacing each aromatic amino acid with Ala in silico and subtracting the calculated CD spectrum from that for the wild-type protein (*19*). Given the strict geometrical requirements of the exciton effect, aromatic exciton couplets are anticipated to be extraordinarily sensitive to local structural perturbations that might well be introduced during the experimental modification of any given protein structure. A considerable degree of untapped potential lies in the identification and application of aromatic exciton interactions to study protein function in the current era of structural proteomics. In this paper, we report evidence of the modulation of an aromatic exciton couplet in a lipid-metabolizing integral membrane enzyme.

We have been investigating the structure and function of PagP, a 161-amino acid membrane protein that resides within the outer membranes of pathogenic Gram-negative bacteria such as *Escherichia coli* (*20*). PagP is an enzyme of lipid metabolism that transfers a palmitate chain from a phospholipid molecule to the lipid A (endotoxin) component of lipopolysaccharide (LPS) (*21*). The Gram-negative outer membrane is an asymmetric bilayer that normally displays LPS in the outer leaflet and restricts phospholipids to the inner leaflet (*22*). This asymmetric lipid organization creates a permeability barrier to hydrophobic antibiotics and detergents that are normally encountered in the host and natural environments (*23*). PagP provides bacteria with a degree of resistance to host-derived antimicrobial agents and attenuates the ability of endotoxin to activate the TLR-4 host defense pathway (*24*, *25*). Additionally, PagP can function as an apical sensory transducer that reports perturbations of lipid asymmetry by a novel signal transduction mechanism in bacteria (S. Kim, W. Jia, E. Vinogradov, C. Gyles, and R. Bishop, unpublished observations).

PagP is an eight-stranded antiparallel β-barrel with a short α-helix at its N-terminus, and it sits in the membrane with the barrel axis tilted by roughly 25° (Figure 1A) (*11*). The PagP palmitate recognition pocket, known as the hydrocarbon ruler, resides within the interior of the β-barrel and is localized in the outer LPS-exposed region of the protein (*11*). A single molecule of the detergent lauroyldimethylamine *N*-oxide (LDAO) serves to identify the position of the hydrocarbon ruler within the β-barrel interior (Figure 1A). Two discontinuities in β-strand hydrogen bonding within this LPS-exposed region provide obvious routes for lateral access of lipids to the hydrocarbon ruler (*10*, *26*). The implication that PagP depends on the aberrant migration of phospholipids into the outer leaflet is supported by observations that the enzyme normally remains dormant in outer membranes until its activity is directly triggered by perturbations to lipid asymmetry (*27*).

A striking enzymological feature of PagP lies in its ability to distinguish a 16-carbon saturated palmitate chain in phospholipids from all other acyl chains, even those that differ by only a single methylene unit (*11*, *21*). The depth of the PagP hydrocarbon ruler, which is lined at its base by Gly88, determines this single-methylene unit resolution (Figure 1B). PagP lacks any Cys residues, but it is particularly rich in aromatic amino acids and includes 10 Phe, 11 Tyr, and 12 Trp residues, not including the N-terminal signal peptide. During our efforts to modulate acyl-chain selection by site-specific chemical methylation of a Gly88Cys PagP mutant, we have discovered an exciton couplet that could be pinpointed to an interaction between Tyr26 and Trp66 at the floor of the hydrocarbon ruler. We demonstrate that this intrinsic exciton probe can provide a gauge for reporting methylene unit resolution in the PagP hydrocarbon ruler.

---

[1] Abbreviations: CD, circular dichroism; DSC, differential scanning calorimetry; ESI-MS, electrospray ionization mass spectrometry; LDAO, lauroyldimethylamine *N*-oxide; LPS, lipopolysaccharide; MNBS, methyl *p*-nitrobenzenesulfonate.
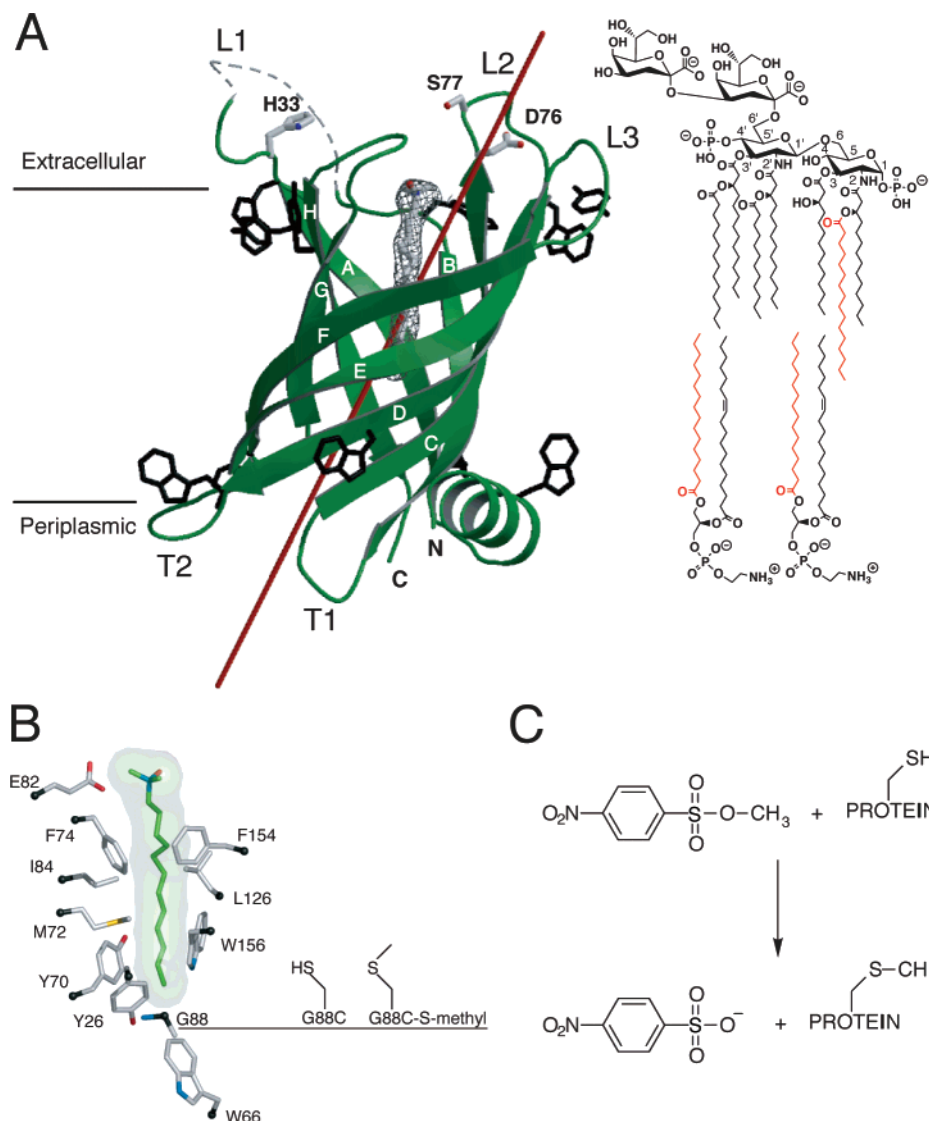
FIGURE 1: Site-specific chemical modification of the PagP hydrocarbon ruler. (A) PagP resides in the *E. coli* outer membrane, where LPS (shown as Kdo$_2$-lipid A) lines the outer leaflet and phospholipids line the inner leaflet. A bound LDAO detergent molecule resides within the PagP hydrocarbon ruler, which has lateral access to lipid substrates in the outer leaflet. PagP transfers a palmitate chain (red) from a phospholipid to lipid A and depends on the aberrant migration of phospholipids into the outer leaflet. (B) The hydrocarbon ruler dimensions determine PagP's ability to strictly select a 16-carbon saturated palmitate chain. Substitution of Gly88 at the base of the hydrocarbon ruler can cause PagP to select shorter acyl chains. (C) Strategy for site-specific S-methylation of Gly88Cys PagP using MNBS.

EXPERIMENTAL PROCEDURES

Expression and Purification of PagP. To purify PagP in a denatured state, we expressed it without its native signal peptide in *E. coli* BL21(DE3) transformed with the plasmid pETCrcAHΔS or its mutant derivatives that were constructed using the QuickChange protocol (Stratagene) as described previously (*10*). All oligonucleotide primers used in our mutagenesis and cloning procedures are identified in Table S1 of the Supporting Information. Bacteria were cultured in 1 L of Luria-Bertani medium supplemented with ampicillin at 100 μg/mL and grown to an optical density at 600 nm of 0.50 and then induced with 1 mM isopropyl β-D-thiogalactopyranoside for 3 h. The induced cells were harvested, suspended in 20 mL of 50 mM Tris-HCl (pH 8.0) and 5.0 mM EDTA, and broken by being passed twice through a French pressure cell at 10 000 psi, and the insoluble material was recovered by centrifugation in a Beckman MLA-80 rotor at 27 000 rpm and 4 °C for 20 min using an Optima MAX-E ultracentrifuge. The pellets were washed

in 20 mL of 50 mM Tris-HCl (pH 8.0) and 2% Triton X-100 followed by 20 mL of 50 mM Tris-HCl (pH 8.0) and then solubilized in 10 mL of 50 mM Tris-HCl (pH 8.0) and 6 M Gdn-HCl. Supernatants were collected after centrifugation and loaded onto a 5 mL bed of His-bind resin (Novagen) that was charged with 50 mM NiSO$_4$ and equilibrated with 3 column volumes of 10 mM Tris-HCl (pH 8.0), 250 mM NaCl, 6 M Gdn-HCl, and 5 mM imidazole. The sample was applied to the column and washed with 10 column volumes of the equilibration buffer, followed by 5 column volumes of 10 mM Tris-HCl (pH 8.0), 250 mM NaCl, 6 M Gdn-HCl, and 20 mM imidazole. The samples were eluted in a step gradient using 5 mL each of 35, 50, 75, 100, and 125 mM imidazole. SDS−PAGE confirmed the presence of purified PagP in the 100 and 125 mM imidazole fractions, which were pooled and dialyzed against distilled water, and the precipitated protein was collected. The protein was resuspended in 8.8 mL of 8 M Gdn-HCl and 0.34 M Tris-HCl (pH 8.6), and the concentration of the purified wild-

type protein was determined, using a calculated extinction coefficient (ϵ_{280}) of 82 630 M^{-1} cm^{-1}, to be 6.67 mg/mL for a total yield of 58.7 mg (*28*). The remaining mutant proteins were obtained in similar yields.

PagP Trp66 mutant proteins that failed to refold in vitro could be folded in vivo when they were expressed with the intact signal peptide in plasmid pETCrcAH and then purified directly from LDAO-solubilized membranes in 1 mg quantities from 1 L cultures as described previously (*21*).

Methylation of PagP. Wild-type and Gly88Cys mutant PagP in Gdn-HCl were subjected to an S-methylation procedure using methyl *p*-nitrobenzenesulfonate (MNBS) (*29*). Control reaction mixtures excluding only MNBS were also prepared, and the four reactions were carried out in capped glass tubes. Protein in 8 M Gdn-HCl and 0.34 M Tris-HCl (pH 8.6) was adjusted to 5 mg/mL in a final volume of 5 mL containing 6 M Gdn-HCl, 0.25 M Tris-HCl (pH 8.6), 3.3 mM EDTA, and 25% (v/v) acetonitrile. The solutions were flushed with N$_2$ for 1 min to create an anoxic barrier, and 50 μL of 260 mM β-mercaptoethanol was added (10−50-fold molar excess of the protein). The tubes were tightly sealed, placed in a 50 °C bath for 1 h, and then gradually cooled to 37 °C. Under the N$_2$ barrier, 0.5 mL of 5.2 mM MNBS (2-fold molar excess of the β-mercaptoethanol) was added, and the tubes were tightly sealed and placed in a 37 °C bath for 2 h. The reactions were quenched via addition of 5 μL of 14 M β-mercaptoethanol. The reaction mix was dialyzed exhaustively against distilled water, and the precipitated proteins were collected and dissolved in 10 mL of 10 mM Tris-HCl (pH 8.0) and 6 M Gdn-HCl. The protein yield was nearly quantitative (25 mg) for all four samples. An aliquot of each sample (0.5 mL) was dialyzed against water and the precipitated protein used for mass spectrometry.

Electrospray Ionizatation Mass Spectrometry (ESI-MS). MS was performed at the Advanced Proteomics Facility at the Hospital for Sick Children. Our procedure for dissolving precipitated PagP was adapted from a prior study of lactose permease (*30*). Precipitated samples to be analyzed were dissolved in 5 mL of a 1:1 (v/v) acetonitrile/1% formic acid mixture at a concentration of ~1 ng/μL just prior to ESI-MS and were injected directly into a triple-quadrupole mass spectrometer. The positive ion mode was used and the cone potential maintained at 48 eV and the collision energy at 4 eV. The spectra were reconstructed using Mass Lynx 3.5. In one instance, a Sciex API III$^+$ triple-quadrupole mass spectrometer was used, but all other analyses were performed with a Micromass Quattro Ultima LC-ESI/APCI triple-quadrupole mass spectrometer.

Refolding of PagP. Samples in 10 mM Tris-HCl (pH 8.0), 6 M Gdn-HCl, and 20 mM β-mercaptoethanol were diluted dropwise (~1 drop per 2 s) into a 10-fold excess of 10 mM Tris-HCl (pH 8.0) and 20 mM β-mercaptoethanol containing 0.5% LDAO at room temperature with vigorous stirring and left to stir overnight at 4 °C. The β-mercaptoethanol was excluded in subsequent refolding experiments using PagP mutants that lack any Cys residues. The refolding sample was then applied to a 4 mL bed of His-bind resin (Novagen) charged with 50 mM NiSO$_4$ and equilibrated with 10 mM Tris-HCl (pH 8.0), 0.1% LDAO, and 5 mM imidazole. The column was washed with 10 column volumes of the equilibration buffer and 10 column volumes of 10 mM Tris-

HCl (pH 8.0), 0.1% LDAO, and 20 mM imidazole and then eluted with 2 mL of 10 mM Tris-HCl (pH 8.0), 0.1% LDAO, and 250 mM imidazole. The sample was dialyzed against 10 mM Tris-HCl (pH 8.0) and 0.1% LDAO, and the refolded samples (6 μg) were resolved via SDS−PAGE on 1 mm Novex 16% Tris glycine precast gels under reducing or nonreducing conditions (Invitrogen). The heated samples were boiled at 100 °C for 10 min before loading, and protein was stained using Coomassie blue dye. Disulfide bonds were encouraged to form under nonreducing conditions by uncapping the heated and unheated samples on the bench for several hours prior to loading on the gel. Refolded PagP protein concentrations were determined using either the bicinchoninic acid assay (*31*) or by absorbance using an extinction coefficient (ϵ_{280}) determined experimentally by the Edelhoch method (*32, 33*).

CD Spectroscopy. Samples to be analyzed for CD were maintained at a concentration of 0.3−0.1 mg/mL in 10 mM Tris-HCl (pH 8.0) and 0.1% LDAO and were analyzed using a cuvette with a path length of 1 mm. The samples were analyzed with either a Jasco J-812 or an Aviv 215 CD spectrometer, each of which was linked to Peltier devices for temperature control. For each sample, three accumulations were averaged at a data pitch of 1 nm and a scanning speed of 10 nm/min. The temperature was maintained at 25 °C, and data sets were obtained from 200 to 280 nm. For thermal denaturation profiles, samples at a concentration of 0.8−0.3 mg/mL in 10 mM Tris-HCl (pH 8.0) and 0.1% LDAO were analyzed in a cuvette with a path length of 1 mm. The samples were heated from 20 to 100 °C at a rate of 2 °C/min, with a response time of 16 s.

Differential Scanning Calorimetry (DSC). The specific heat capacity (C_p) as a function of temperature was obtained in an N-DSC (cell volume of 0.3 mL) at a scan rate of 1.0 °C/min and a pressure of ~37 psi. The protein sample was first dialyzed overnight at 4 °C against 100 mM sodium phosphate buffer (pH 8.0) with 0.05% LDAO. The solution was then degassed for 5 min before it was loaded into the DSC cells. A blank scan with buffer in both calorimeter cells was subtracted to correct for the difference between the cells. The DSC instrument that was employed was a CSC model 6100 Nano II. The software used to collect the data was DSCRUN, N-DSC control program (version 2.5.0.29s), Calorimetry Science Corp. The software used to visualize the data was cpcalc (version 2.1, Applied Thermodynamics), while the software used to process the data was Microcal TM (version 5.0, Microcal Software Inc.).

Theoretical Calculations of CD. The CD spectrum for wild-type PagP was calculated using the X-ray structure (*11*) (PDB entry 1THQ). The methods and parameters have been described previously (*18, 34*). Calculations were also performed for mutants generated in silico by deletion, one by one, of each of the Tyr and Trp side chains in the vicinity of Gly88 in the crystal structure: Tyr26, Trp60, Trp66, Tyr70, Tyr87, and Trp156. (Phe side chains were not mutated because they have only the weak 260 nm band above 220 nm.) In each case, a difference spectrum was calculated by subtracting the predicted spectrum of the mutant from that of the wild type, thus providing the contribution of the mutated side chain to the wild-type CD spectrum.

Hydrocarbon Ruler Assays. Kdo$_2$-lipid A was prepared from heptose-deficient *E. coli* WBB06 as described previ-

ously (*35*) and quantified as described (*36*). Synthetic diacylphosphatidylcholines were obtained from Avanti Polar Lipids (Alabaster, AL). The hydrocarbon ruler assays were performed at 30 °C by a TLC-based radiolabeling procedure as described previously (*11*), except that 25 μCi of [^{32}P]-orthophosphate was employed in place of sodium [^{14}C]-acetate.

Molecular Dynamics. We have used high-temperature simulated annealing to probe the local conformational changes induced by mutation of Gly88. The same procedure has been applied to two starting conformations. The initial conformation was the X-ray structure (*11*) (PDB entry 1THQ) in the absence of LDAO and crystal waters. Another starting conformation was obtained by equilibration of the X-ray structure containing a rebuilt L1 loop and bound LDAO, and embedded in an explicit 1,2-dimyristoyl-*sn*-glycero-3-phosphocholine (*37*) bilayer and TIP3P water (*38*). All nonprotein atoms were then removed. Residues His22 and His102 were protonated on $N^{\delta 1}$, while residues His33 and His67 were protonated on $N^{\epsilon 2}$. All simulations were carried out using the CHARMM software package(*39*) using the CHARMM22 all-hydrogen topology and parameter files (*40*). Parameters for the methylated cysteine residue were developed on the basis of methionine via removal of C^{β}. All nonbonded interactions (Lennard-Jones and Coulombic) were switched off from 10 to 11 Å. The neglect of long-range electrostatic interactions is justified because conformational sampling is restricted to local side-chain rearrangements of neutral residues within a static protein framework.

Initial conformations of the mutants were obtained as follows. Hydrogen atoms to be replaced by heavy atoms were chosen such that the nascent side chain was in the LDAO binding pocket and pointed toward the extracellular region. Mutants were created according to the following succession: Gly88Ala ($H^{\alpha 1} \rightarrow C^{\beta}$, $H^{\alpha 2} \rightarrow H^{\alpha}$), Ala88Cys ($H^{\beta 3} \rightarrow S^{\gamma}$), Cys88-*S*-methyl ($H^{\gamma} \rightarrow C^{\delta}$), and Cys-*S*-methyl88Met ($S^{\gamma} \rightarrow C^{\gamma}$, $C^{\delta} \rightarrow S^{\delta}$, $H^{\delta 1} \rightarrow C^{\epsilon}$). A harmonic restraining potential was applied for C′, N′, C^{α}, and O′ atoms of residue 88 with a force constant of 10 kcal mol^{-1} Å^{-2}, and all other residues were held fixed. Each mutant was energy minimized.

In the remaining calculations, a harmonic restraining potential was applied to the backbone heavy atoms of residues Trp66, Gly68, Tyr70, X88, Thr108, and Leu128 with a force constant of 10 kcal mol^{-1} Å^{-2} (greater by 1 order of magnitude for calculations starting from the X-ray structure). All other residues were held fixed. Each of the conformations resulting from the procedure outlined above was simulated at 3000 K for 75 ps. The temperature was controlled by Langevin dynamics with a friction coefficient of 2.0 ps^{-1}. High-temperature seed conformations were taken after 15, 25, 35, 45, 55, 65, and 75 ps. Each seed was then cooled to 206 K over a minimum of 1.3 ns by reducing the temperature to 0.8 of its previous value after each segment. Dynamics at and below 3000 K were produced with time steps of 0.5 and 1.0 fs, respectively. The final cooling step was followed by energy minimization.

Figures were generated with VMD version 1.8.3 (*41*) and rendered with POV-Ray version 3.6 (Persistence of Vision Pty. Ltd.). Trp66 and X88 are overlaid for all seven replicas. Contouring of the β-barrel interior was performed by HOLE with a cutoff radius of 1.4 Å (*42*). For the wild type and each mutant, contours were generated on the basis of the

initial wild-type structure plus the coordinates of residue 88 overlaid from all seven replicas. All other figures derived from the PagP crystal structure coordinates were rendered using PyMOL (*43*).

RESULTS

In our prior investigation, we analyzed membrane-derived wild-type PagP and its site-specific mutants Gly88Ala, Gly88Cys, and Gly88Met (*11*). To improve the quality of these initial studies, we removed the signal peptide from each of the mutant proteins for expression and purification in a denatured state to be followed by refolding. Since PagP lacks any Cys residues, the single Cys in Gly88Cys PagP was available for a chemical methylation procedure that occurs in Gdn-HCl needed to unfold PagP, which is necessary to expose the Cys residue and to normalize the reactivity of other functional groups (*29*) (Figure 1B,C). By synthesizing Gly88Cys-*S*-methyl PagP, we predicted that we could create a suite of hydrocarbon ruler mutants that select 15-carbon (Gly88Ala), 14-carbon (Gly88Cys), 13-carbon (Gly88Cys-*S*-methyl), and 12-carbon (Gly88Met) saturated acyl chains. The hydrocarbon ruler hypothesis predicts that the substituted amino acid side chain at position 88 will plug the floor of the hydrocarbon ruler and make it shallower by the same length as the introduced side chain. This change in hydrocarbon ruler dimensions should afford a corresponding shortening of the acyl chain that is selected in enzymatic assays.

Site-Specific Chemical Modification of Gly88Cys PagP. We subjected the unfolded wild-type and Gly88Cys PagP proteins to methylation with MNBS (Figure 1C) as described previously (*29*). Control reactions were also performed without MNBS. To detect the incorporation of a single methylene group (14.03 Da) into an ~20 kDa protein, we chose to determine the mass by ESI-MS. This method is incompatible with the Gdn-HCl or LDAO used to keep PagP in solution, but we were able to develop a mild procedure, adapted from a much harsher one using formic acid to perform ESI-MS on lactose permease (*30*); our adaptation involves removing denaturants by dialysis against water and dissolving the precipitated protein in a 1:1 acetonitrile/1% formic acid solution immediately prior to ESI-MS analysis. We could demonstrate that MNBS leads to a 14 Da increase in the mass of the Gly88Cys mutant, but not in the wild-type protein, which lacks any Cys residues (Table 1). The mass spectra reveal that the Gly88Cys mutant in the absence of MNBS treatment forms two species, the major one being a disulfide-linked dimer (Figure 2). MNBS treatment of the Gly88Cys mutant reveals a single molecular species corresponding to a monomeric S-methylated protein. These findings validate the claim that the methylation procedure is both quantitative and highly selective for Cys under the specified conditions (*29*). We were also able to verify the masses of the remaining PagP mutants by ESI-MS (Table 1).

Evaluation of PagP Refolding. The unfolded PagP variants were refolded by dilution into LDAO and evaluated by a qualitative SDS−PAGE assay (Figure 3). Many outer membrane proteins like PagP exhibit the phenomenon of heat modifiability on SDS−PAGE. In these gels, the unheated form of PagP appears folded and more compact as it migrates

Table 1: Selective S-Methylation of Gly88Cys PagP Treated with MNBS

PagP protein[a]	theoretical mass (Da)	ESI-MS (Da)
Gly88Cys control	20221.58	20220.15 ± 0.6
(Gly88Cys S−S dimer)	(40441.14)	(40439.32 ± 1.0)
Gly88Cys with MNBS	20235.61	20234.53 ± 0.5
Δ with S-methyl	14.03	14.38 ± 1.1
wild-type control	20175.49	20174.53 ± 0.4
wild type with MNBS	20175.49	20174.57 ± 0.4
Δ with S-methyl	0	−0.04 ± 0.7
Gly88Ala	20189.52	20190.63 ± 1.7
Gly88Met	20249.64	20249.41 ± 0.7
Tyr26Phe	20159.49	20161.80 ± 2.3
Trp66Phe	20136.45	20135.17 ± 1.9
Trp66His	20126.42	20128.01 ± 2.2

[a] The wild-type *E. coli* PagP protein used in this study lacks the N-terminal signal peptide and contains a C-terminal His$_6$ tag. The amino acid sequence with Gly88 underlined is as follows: MNADEWMT-TFRENIAQTWQQPEHYDLYIPAITWHARFAYDKEKTDRYNE R-PWGGGFGLSRWDEKGNWHGLYAMAFKDSWNKWEPIAGYG-WESTWRPLADENFHLGLGFTAGVTARDNWNYIPLPVLLPLA-SVGYGPVTFQMTYIPGTYNNGNVYFAWMRFQFLEHHHHHH.
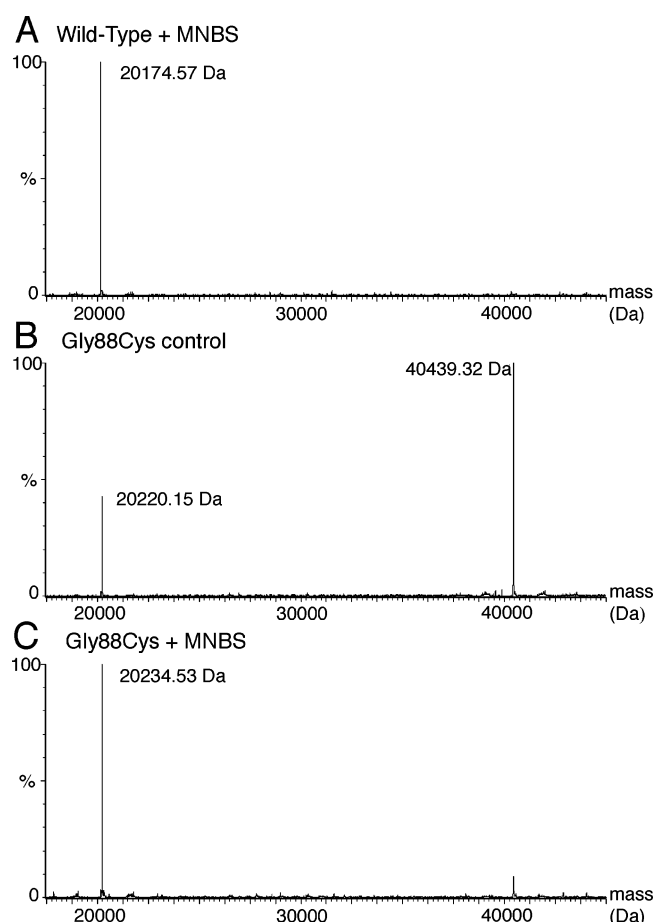

FIGURE 2: ESI-MS confirmation of Gly88Cys-*S*-methyl PagP. (A) Wild-type PagP treated with MNBS exhibits a single mass that corresponds to an unmodified monomeric species. (B) In the absence of MNBS, Gly88Cys PagP exhibits two masses that correspond to an unmodified monomer and a disulfide-linked dimer. (C) MNBS treatment of Gly88Cys PagP results in a 14 Da mass increase for the monomeric species and a loss of the disulfide-linked dimer.

slightly ahead of its expected molecular mass of 20 kDa (*21*). However, after irreversible heat denaturation, PagP migrates at its expected molecular mass. This explanation for the
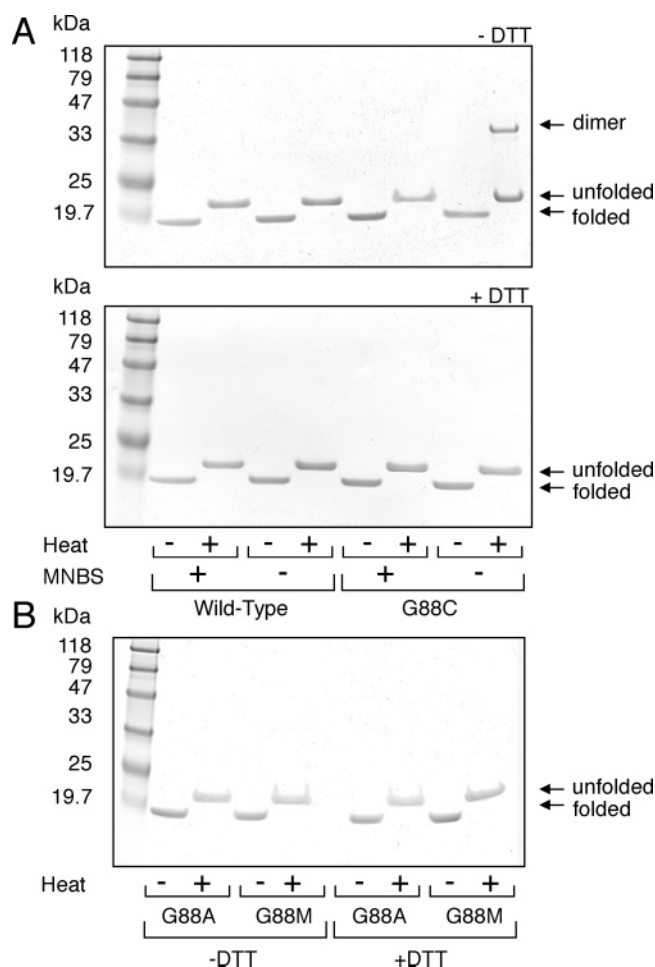

FIGURE 3: SDS−PAGE analysis of PagP refolding. PagP requires heat treatment to become denatured via SDS−PAGE and migrates anomalously fast in the absence of heat treatment. (A) Analysis of wild-type and Gly88Cys PagP under reducing and nonreducing conditions, in the presence and absence of heat treatment, and with or without prior exposure to MNBS. (B) Analysis of Gly88Ala and Gly88Met PagP as described above, but without exposure to MNBS.

observed heat modifiability is reinforced by the observation that only the heat-denatured Gly88Cys PagP is capable of migrating as a disulfide-linked dimer in the nonreducing gel (Figure 3A). The single Cys in this mutant appears to be unexposed in the unheated sample, consistent with the faster-migrating species reflecting a folded state of the protein. Wild-type PagP and its Gly88 mutant derivatives all appeared to be adequately folded by this SDS−PAGE criterion.

Spectroscopic Examination of Refolded PagP Mutants. We wanted to determine whether subtler structural details could be ascertained by a more refined CD spectroscopic examination of the refolded PagP proteins. The LDAO micelles are transparent down to 200 nm in CD analysis of the refolded PagP proteins. The far-UV CD spectrum of wild-type PagP (Figure 4A,B) displays a negative CD band at 218 nm that is characteristic of the n → π* transition derived from peptide bonds in a largely β-sheet conformation (*44*). This observation is consistent with the β-barrel structure of PagP. However, the positive ellipticity at 232 nm is likely the first Cotton effect of an exciton couplet, which becomes fully apparent only by its absence in Gly88Cys PagP (Figure 4A). The second Cotton effect of this exciton couplet is largely superimposed on the β-sheet n → π* transition. The Gly88Cys PagP sulfhydryl group appears to be responsible
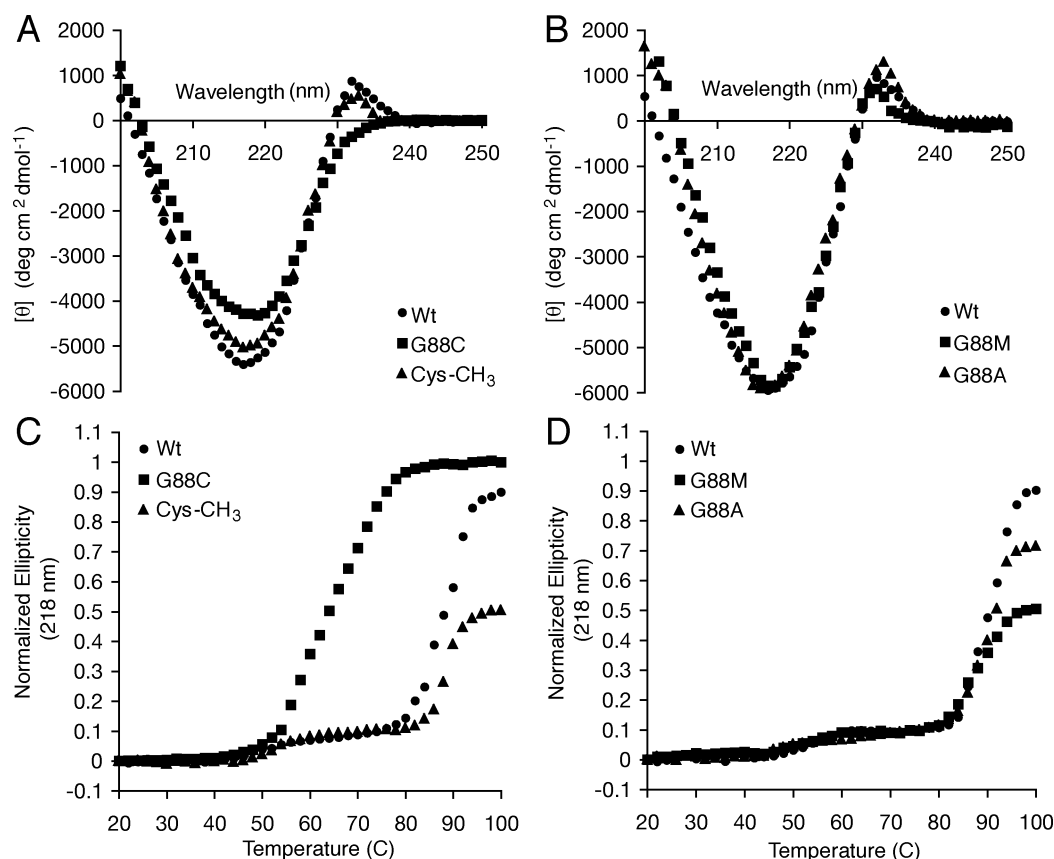
FIGURE 4: Spectroscopic analysis of refolded PagP variants and evaluation of thermal stability. (A and B) Far-UV CD spectra of refolded PagP variants. (C and D) Thermal unfolding profiles of refolded PagP variants assessed by following the loss of the negative ellipticity maximum at 218 nm observed in panels A and B.

for extinguishing the exciton couplet, because Gly88Cys-*S*-methyl PagP restores the exciton couplet to its full strength. The far-UV CD spectra of Gly88Ala and Gly88Met PagP similarly exhibit a robust exciton couplet (Figure 4B).

We reasoned that the absence of the exciton couplet in Gly88Cys PagP might result from a local structural perturbation arising from the sulfhydryl group. We followed loss of the negative ellipticity maximum at 218 nm in thermal unfolding experiments using wild-type PagP and its hydrocarbon ruler mutants (Figure 4C,D). PagP was unfolded irreversibly in these experiments because it precipitated after incubation at 100 °C. However, the proteins that exhibit the exciton couplet all share a thermal denaturation temperature near 88 °C, while Gly88Cys PagP denatures near 65 °C (Figure 4 C). The smaller perturbation apparent near 50 °C in all but Gly88Cys PagP likely represents loss of the excitonic Cotton effect that contributes to the ellipticity at 218 nm because a transition of a similar magnitude is also observed near 50 °C by following the loss of the associated positive ellipticity at 232 nm (Figure 5A). This finding suggests that the exciton is much more sensitive to heat, disappearing at a temperature that is easily tolerated by the β-barrel structure. The transition at 88 °C most likely represents protein unfolding because wild-type PagP was shown to exhibit a thermal transition at the same temperature in a DSC experiment (Figure 5B).

Far-UV CD spectra recorded at high temperatures validate the disappearance of the excitonic signature prior to protein unfolding and reveal that residual β-structure remains at 92 °C (Figure 5C). Precipitation ensuing at higher temper-

atures is consistent with the formation of intermolecular β-structure that would compensate for intramolecular β-structure lost during β-barrel unfolding, because both structures exhibit negative ellipticity at 218 nm. Consequently, the different plateaus reached at high temperatures by the various mutants (Figure 4C,D) likely reflect different tendencies to form intermolecular β-structure in the denatured state. Compared to wild-type PagP, more extensive residual ellipticity is apparent at 92 °C in Gly88Cys-*S*-methyl PagP (Figure S1A of the Supporting Information), which is consistent with its lower plateau as observed in Figure 4C. In contrast to the aggregation observed in LDAO at high temperatures, a distinct conformation is indicated after heat denaturation in the presence of 1% SDS because we previously observed that heat-denatured PagP migrates in a monodisperse state via SDS−PAGE (Figure 3). We find that PagP retains the apparent excitonic signature associated with its β-barrel structure after dilution into 1% SDS at room temperature, but boiling the sample over the course of 1 h followed by cooling to room temperature reveals characteristics of an α-helical protein in far-UV CD spectra (Figure 5D). Helix formation in SDS is also indicated as a function of increasing temperature (Figure S1B of the Supporting Information) by a gradual increase in rotational strength, an associated red shift of the amide n → π* transition from 218 to 222 nm, and the acquisition of a new negative ellipticity maximum at 208 nm, which arises from exciton splitting of the amide π → π* transition.

Theoretical Exciton Analysis. To pinpoint any aromatic amino acid residues that contribute to the observed exciton
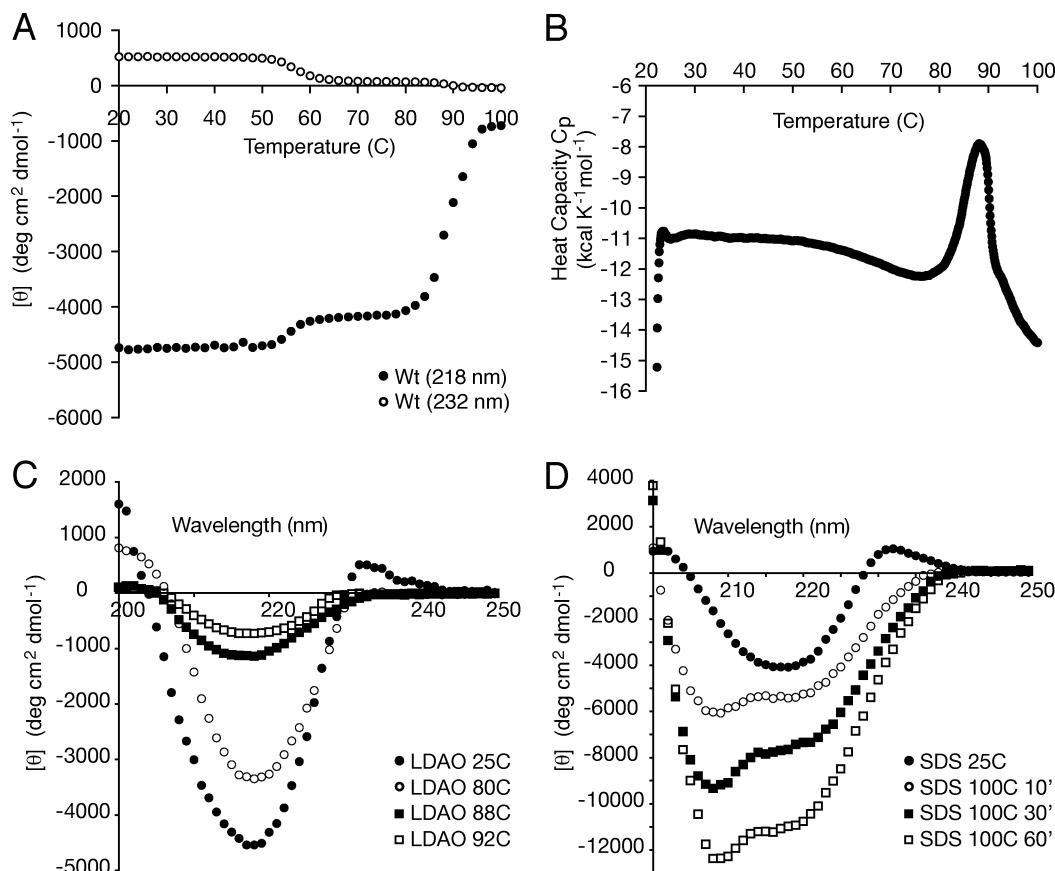
FIGURE 5: Secondary structure associated with thermal unfolding of wild-type PagP. (A) Thermal unfolding profile of refolded wild-type PagP assessed by following the loss of the ellipticities at 218 and 232 nm. (B) Thermal unfolding profile of wild-type PagP assessed by DSC. (C and D) Far-UV CD spectra of wild-type PagP refolded in LDAO and recorded at various points along the thermal unfolding profile after a 15 min equilibration (C) and in the presence of 1% SDS as a function of the time of incubation at 100 °C (D).

couplet, we used the high-resolution PagP crystal structure coordinates (*11*) (PDB entry 1THQ) to predict the CD spectrum (Figure S3A of the Supporting Information). We were encouraged to find that calculations using standard methods and parameters (*18*, *34*) reproduced the experimental positive CD band at 232 nm (predicted $[\theta]_{max} = 1500$ at 237 nm). Analysis of the band responsible for this positive feature shows that it is located at 232 nm and is largely due to the 230 nm band of Tyr26 (69%) and the 225 nm band of Trp66 (21%), with contributions of 1−3% from Trp60, Tyr70, Tyr87, and Trp156. This analysis was supported by calculations on in silico mutants in which Tyr26, Trp66, and other participants in the long-wavelength positive band were deleted. Deletion of Tyr26 gave negative CD throughout the 220−240 nm region, and the difference spectrum of Tyr26Ala with the wild type exhibited a positive exciton couplet centered at 227 nm (Figure S3B of the Supporting Information). Deletion of Trp66 gave a spectrum with a weak positive maximum at 238 nm, with only 20% of the wild-type intensity, and the difference spectrum for Trp66Ala was a positive couplet comparable in magnitude to that for Tyr26Ala (Figure S3A of the Supporting Information). For the other mutants, the long-wavelength positive band persisted, with nearly constant contributions from Tyr26 and Trp66. The magnitude of the band was changed only slightly upon deletion of Trp60 or Tyr70 (Figure S3E,F of the Supporting Information). However, deletion of Tyr87 led to a 70% increase in amplitude, whereas deletion of Trp156 led to a 50% decrease (Figure S3C,D of the Supporting

Information). These two side chains make significant but opposing contributions to the long-wavelength exciton band, despite their low fractional participation. Nevertheless, Tyr26 and Trp66 dominate the 232 nm exciton band, and any perturbation that eliminates this band must affect one or both of these side chains. Therefore, exciton theory applied to the PagP crystal structure has conclusively identified Tyr26 and Trp66 as the main interacting aromatic side chains responsible for the observed exciton couplet.

The structural relationship between the hydrocarbon ruler and the nondegenerate Tyr26−Trp66 exciton pair is shown to indicate how the exciton effect arises from an interaction between $\pi \rightarrow \pi^*$ transitions with similar but distinct energies (Figure 6A). The ^1L_a and ^1B_b electric dipole transition moments in Tyr26 and Trp66, respectively, couple to give two exciton states separated by the splitting energy, $\Delta_{ij} = (\delta_{ij}^2 + 4V_{ij}^2)^{1/2}$, where δ_{ij} is the energy difference between the two transitions, σ_i and σ_j, and V_{ij} is the interaction (Davydov) energy (Figure 6B). Considering only the coupling between the Tyr26 ^1L_a band and the Trp66 ^1B_b band, and using the monopole−monopole interaction energy for calculating the wavelengths and the rotational strengths, the resulting exciton couplet is predicted to be positive and to exhibit a peak-to-trough strength of ~2500 deg cm^2 dmol^{-1} (Figure 6 C). The sign of an exciton couplet is defined in accordance with the long-wavelength (first) Cotton effect and will be reversed in the enantiomeric structure. In contrast to the degenerate exciton case (with two identical chromophores), where Δ_{ij} reduces to $2V_{ij}$, the mixing of the Tyr26
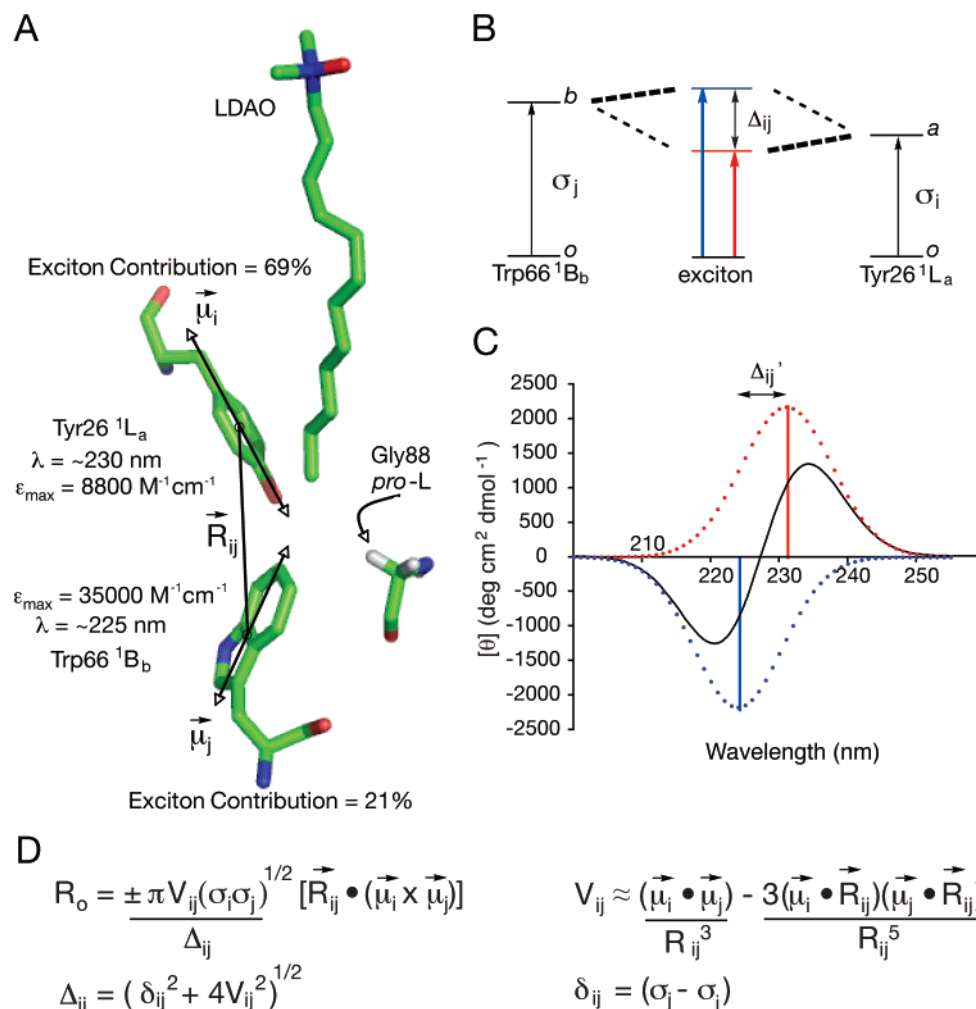
FIGURE 6: Theoretical analysis of a nondegenerate exciton interaction in PagP. (A) Structural relationships between the PagP hydrocarbon ruler, emphasizing the LDAO molecule and the *pro*-L hydrogen of Gly88, and the exciton interaction between Tyr26 and Trp66. The polarization axes for the interacting Tyr26 ^1L_a (μ_i) and Trp66 ^1B_b (μ_j) electric dipole transition moment vectors are shown to emphasize their relationships with the interchromophore distance vector R_{ij}. Key absorption parameters and the calculated exciton contribution to the wild-type PagP far-UV CD spectrum are also shown. (B) The $\pi \rightarrow \pi^*$ transitions from ground states *o* to excited states *a* (for Tyr26 ^1L_a) or *b* (for Trp66 ^1B_b) are split by a nondegenerate exciton interaction into two new exciton states, which generate CD Cotton effects equal in magnitude, opposite in sign, and separated by the splitting energy Δ_{ij}. This splitting energy is given by $(\delta_{ij}^2 + 4V_{ij}^2)^{1/2}$, where δ_{ij} ($=\sigma_j - \sigma_i$) is the difference in the transition energies of the two chromophores and V_{ij} is the energy of interaction between the transition moments. Tyr26 and Trp66 each dominate the low-energy (red) and high-energy (blue) exciton states, respectively. (C) The exciton couplet (solid line) calculated from the Tyr26−Trp66 exciton interaction is the resultant of the two exciton-split CD Cotton effects (red and blue dotted curves), which are separated on the wavelength scale by Δ_{ij}', the wavelength equivalent of Δ_{ij}. (D) The theoretical rotational strengths (R_o) of nondegenerate exciton split CD Cotton effects are proportional to V_{ij}, Δ_{ij}, and a scalar triple product involving the vector connecting the centers of the two transitions and the dipole transition moments. V_{ij} can be approximated by the point-dipole approximation, but a more exact method is used in calculating the spectra shown here.

^1L_a and Trp66 ^1B_b bands is incomplete. The Tyr26 ^1L_a band dominates the long-wavelength Cotton effect, and the Trp66 ^1B_b band dominates the short-wavelength Cotton effect. The exciton couplet will disappear in CD when either V_{ij} or the rotational strength (R_o), representing the area under the two Gaussian distributions, is zero (*12*). Although the point-dipole approximation for calculating V_{ij} is only accurate when the interchromophore distance vector R_{ij} is large compared to the dimensions of the interacting chromophores and is replaced in practice by a monopole (distributed dipole) approximation (*19*), it usefully illustrates how V_{ij} is related to the electric dipole transition moment vectors for μ_i and μ_j (Figure 6D). The dot products dictate that V_{ij} is maximized by parallel and minimized by orthogonal vector relationships. In contrast, the scalar triple product in R_o for a nondegenerate exciton interaction dictates that R_o is maximized by orthogo-

nal and vanishes for parallel vector relationships (*12*). Theoretically, the exciton can be extinguished by any structural perturbation arising from a Gly88 substitution that induces parallel or orthogonal relationships from the oblique vector relationships normally found to exist between the Tyr26 ^1L_a and Trp66 ^1B_b transitions.

Experimental Exciton Analysis. To experimentally validate the predicted Tyr26−Trp66 nondegenerate exciton in PagP, we constructed, purified, and analyzed the Tyr26Phe, Trp66Phe, and Trp66His mutants. Both Trp66 mutants failed to refold as assessed by SDS−PAGE (Figure 7A), which indicates that Trp66 is a critical determinant of PagP folding. The Trp66His and Trp66Phe mutants remained in solution after failing to refold in LDAO at 25 °C but precipitated after heating to 100 °C; their far-UV CD spectra revealed negative ellipticity below 210 nm at 25 °C, but 218 nm
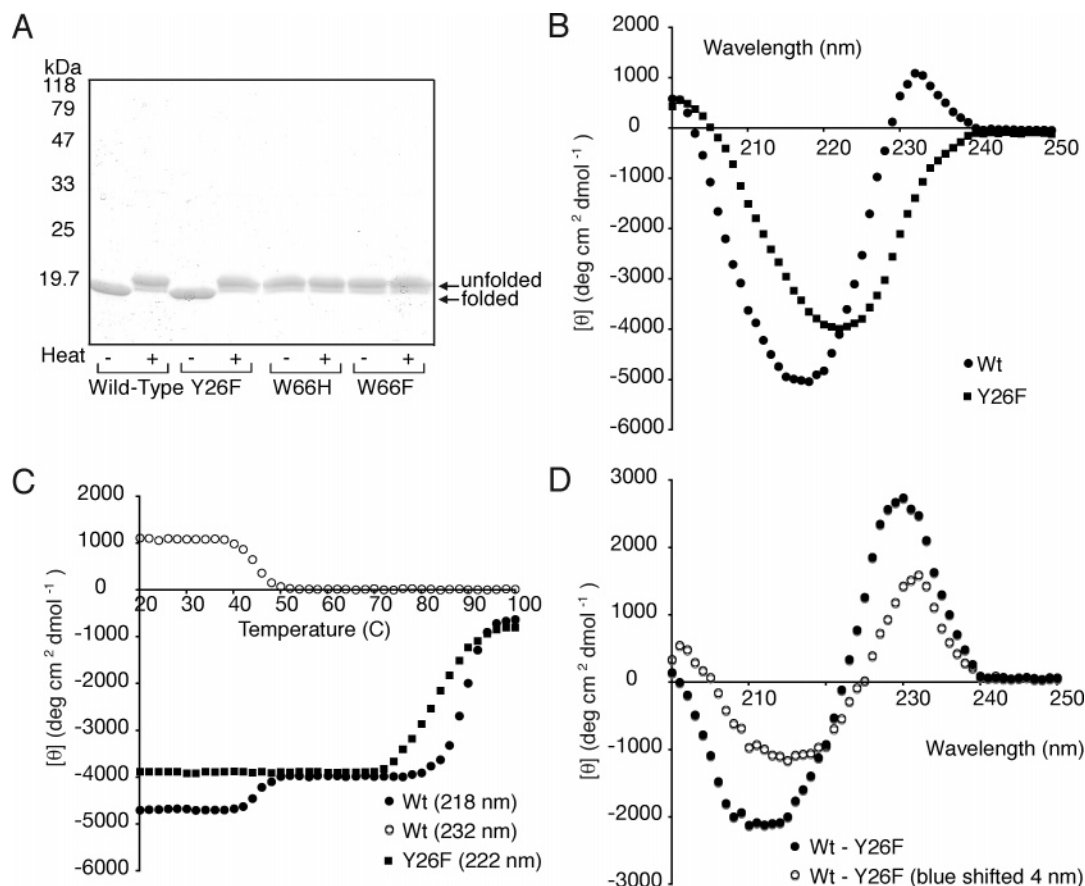
FIGURE 7: Refolding and spectroscopic analysis of PagP exciton mutants. (A) Wild-type PagP and the Tyr26Phe, Trp66Phe, and Trp66His mutants were subjected to refolding in LDAO and evaluated by SDS−PAGE. (B and C) Wild-type PagP and the Tyr26Phe mutant were further analyzed by far-UV CD spectroscopy (B), and the thermal unfolding profiles were obtained by following the loss of the peak ellipticity bands (C). (D) Difference far-UV CD spectra determined by subtracting the Tyr26Phe PagP spectrum, with and without an introduced 4 nm blue shift, from the wild-type spectrum.

negative ellipticity was induced at 92 °C to a similar extent as observed previously for wild-type PagP at the same temperature (Figure S1C of the Supporting Information). This observation supports our suggestion that the residual ellipticity observed at high temperatures reflects intermolecular β-structure formed prior to precipitation. By following the loss of ellipticity at 202 nm and the formation of ellipticity at 218 nm, we found the Trp66 mutants revealed that unfolded PagP in LDAO begins the transition to an aggregated state above 80 °C (Figure S1D of the Supporting Information).

The Tyr26Phe mutant refolded successfully, and its far-UV CD spectrum did not exhibit any positive CD in the 230 nm region, thus confirming the predicted contribution of Tyr26 to the long-wavelength exciton band (Figure 7B). However, the negative band was red-shifted from 218 to 222 nm, which indicates that the peptide backbone conformation is modulated by contributions from Tyr26 because loss of the exciton prior to β-barrel unfolding at 80 °C (Figure 5C), or in the Gly88Cys mutant (Figure 4A), was not accompanied by a red shift. By following loss of the 222 nm negative CD band in Tyr26Phe PagP, we observed an 8 °C reduction in the thermal transition temperature when compared to the 218 nm negative CD band lost from wild-type PagP (Figure 7C); only the latter displays loss of the exciton in the 40−50 °C range, and an apparent contribution of Tyr26 to folding cooperativity is revealed by comparing the slopes of the two precipitation curves. Subtracting the Tyr26Phe far-UV CD

spectrum from that for wild-type PagP reveals the exciton couplet (Figure 7D), but the peak-to-trough strength better matches the theoretical prediction (Figure 6C) when the Tyr26Phe spectrum is first blue-shifted manually back to 218 nm from 222 nm.

Although the Trp66 mutants failed to refold in vitro, we could successfully purify folded Trp66Phe and Trp66His PagP when they were expressed in vivo with an intact signal peptide (Figure S2 of the Supporting Information) as described previously (*21*). The in vivo-folded wild-type and Trp66 mutant PagP proteins appeared folded by both SDS−PAGE and far-UV CD criteria (Figure S2A,B of the Supporting Information). The far-UV CD spectra validate the predicted contribution of Trp66 to the nondegenerate exciton interaction by revealing the loss of positive ellipticity above 230 nm and the formation of a weaker negative ellipticity maximum at 218 nm. In contrast to Tyr26Phe PagP, no red shift was associated with the loss of the exciton in the Trp66 mutants. The predicted dominance of the Tyr26 and Trp66 contributions to the long- and short-wavelength exciton bands, respectively (Figure S3A,B of the Supporting Information), appears to be validated by the experimental observations (Figure 7B and Figure S2B of the Supporting Information). The failure of the Trp66 mutants to fold in vitro is reflected in the instability associated with their reduced thermal unfolding temperature of 75 °C compared with a temperature of 88 °C observed for the in vivo folded wild-type protein (Figure S2C of the Supporting Informa-

tion). However, the Gly88Cys PagP mutant was successfully folded in vitro despite the fact it displays a thermal unfolding temperature of only 65 °C (Figure 4C). Periplasmic chaperones are known to assist the folding of outer membrane β-barrel proteins in *E. coli* and likely help to overcome the folding defect associated with the PagP Trp66 mutations (*45*). The observation of reduced thermal unfolding temperatures for both the Tyr26 (Figure 7C) and Trp66 (Figure S2C of the Supporting Information) PagP mutants suggests that destabilizing effects will likely be associated with proximal groups that perturb these aromatic side chains.

Hydrocarbon Ruler Experiments. The remarkable thermal stability of PagP in detergent micelles provides the destabilized Gly88Cys PagP mutant with sufficient residual stability to easily tolerate the temperature of 30 °C encountered in the PagP hydrocarbon ruler assay. The assays are performed using a suite of synthetic diacylphosphatidylcholine donors that possess saturated acyl chains varying in length from 10 to 18 carbons in single-methylene unit increments (*11*). [^{32}P]Kdo$_2$-lipid A (Figure 1A) is used as the acyl acceptor, and acylation is assessed by a TLC-based assay (Figure 8). All PagP derivatives that exhibit exciton couplets are able to select acyl chains of the length predicted by the hydrocarbon ruler hypothesis, and they do it with single-methylene unit resolution. Only Gly88Cys PagP, which lacks the exciton because of a local structural perturbation arising from its single sulfhydryl group, could not accommodate a single acyl chain of the predicted length. Rather, Gly88Cys PagP accommodated two acyl chains: one with the predicted length and one extended by an extra methylene unit.

In Silico Mutagenesis. Efforts to crystallize the PagP mutant proteins have so far not met with any success. Therefore, we opted to perform in silico mutagenesis and assess the conformational preferences of the substituted side chains by constrained simulated annealing molecular dynamics. The main features surrounding the floor of the hydrocarbon ruler in the wild-type PagP crystal structure are outlined in Figure 6A and given a different perspective in the right portion of Figure 8A. Here the LDAO molecule that occupies the hydrocarbon ruler has been removed, and the vacated space is outlined with a contoured shell. The position of Gly88 reveals that the *pro*-L hydrogen is directed toward the base of the hydrocarbon ruler and should direct any substituted amino acid side chain into the base of the cavity. Flanking this site are Tyr26 and Trp66, which approach each other in a geometric relationship that affords an exciton delocalization of the two chromophore-excited states. The amino acid substitutions associated with expression of both the exciton couplet and single-methylene unit resolution were found to advance into the hydrocarbon ruler floor (Figure 8B,D,E), but the Cys sulfhydryl group was found to recede downward and induce a 1 Å shift in the position of the indole ring of Trp66, which alters its geometric relationship with respect to Tyr26 (Figure 8C). Another possible source of perturbation of the local structure of the enzyme is the presence of a weak electrostatic interaction between the sulfhydryl group and the hydroxyl group of Tyr26, which is 4 Å away. These predictions suggest that the loss of the exciton in Gly88Cys PagP results from a local perturbation of Trp66 and/or Tyr26 arising from the downward orientation of the Cys sulfhydryl group, which

also serves to expand the hydrocarbon ruler and allow the enzyme to accommodate an additional acyl chain with one extra methylene unit. We propose that the Gly88Cys PagP hydrocarbon ruler is tailored to optimally accommodate an acyl chain that lies somewhere between C14 and C15 and is thus capable of using both.

The thioether (sulfide) bond introduced into Gly88Cys-*S*-methyl PagP is a decidedly hydrophobic entity (*46*) that is expected to occupy the hydrophobic pocket as predicted by the hydrocarbon ruler hypothesis. In vitro, this mutant selects the expected 13-carbon saturated acyl chain with single-methylene unit resolution (Figure 8D), and it exhibits a full exciton couplet (Figure 4A). Although the simulated annealing calculations fall short of exhaustively sampling conformational space, the annealed conformations of Gly88Met suggest that this side chain spans a wider spatial distribution than the other mutants of Gly88 (Figure 8A–E). This observation is consistent with the fact that Gly88Met PagP, while preferentially selective for the expected 12-carbon saturated acyl chain, also exhibits residual ability to bind an acyl chain with one extra methylene unit. These observations might reflect a positional preference within the hydrocarbon ruler environment for the inherent conformational flexibility around the thioether CH$_3$S−CH$_2$ torsional unit and/or dispersion forces associated with the thioether sulfur atom (*46*).

Despite our experimental observations that the exciton is retained in all mutants except Gly88Cys PagP, exciton calculations using structures from simulated annealing did not predict its presence in any of them. Even for wild-type PagP, the simulated annealing results are not predicted to have an exciton. This finding suggests that the X-ray conformation is a better representation of the conformational ensemble of the protein than the locally relaxed conformations obtained from our simulated annealing calculations. Obtaining more realistic conformations of the mutants would require letting the enzyme relax and reach thermal equilibrium in explicit membrane and solvent. Nevertheless, the high-temperature simulated annealing calculations are a first step in modeling the local conformational preferences of the mutant side chains. These preferences are qualitatively different for the Cys mutant, which is consistent with the measured extinction of the exciton.

DISCUSSION

Excitons in proteins can arise from through-space interactions between the excited states of neighboring Trp and/or Tyr aromatic chromophores. Although such excitons are by no means present in every protein structure, they are more common than is widely appreciated (*19*). Exciton couplets observed in some proteins have been previously employed to analyze protein structure (*47*, *48*), but efforts to identify the residues actually responsible for the exciton interaction, and to employ them as intrinsic probes for monitoring structure−function relationships, have been rare. An exciton couplet formed by Trp172 and Trp215 in chymotrypsinogen and chymotrypsin was used to demonstrate conversion of the active enzyme conformation to the zymogen conformation at high pH and to show that the diisopropyl fluorophosphate-inactivated enzyme does not undergo this transition (*49*). However, the excitonic origin of the far-UV features in the CD spectra of chymotrypsinogen and chymotrypsin
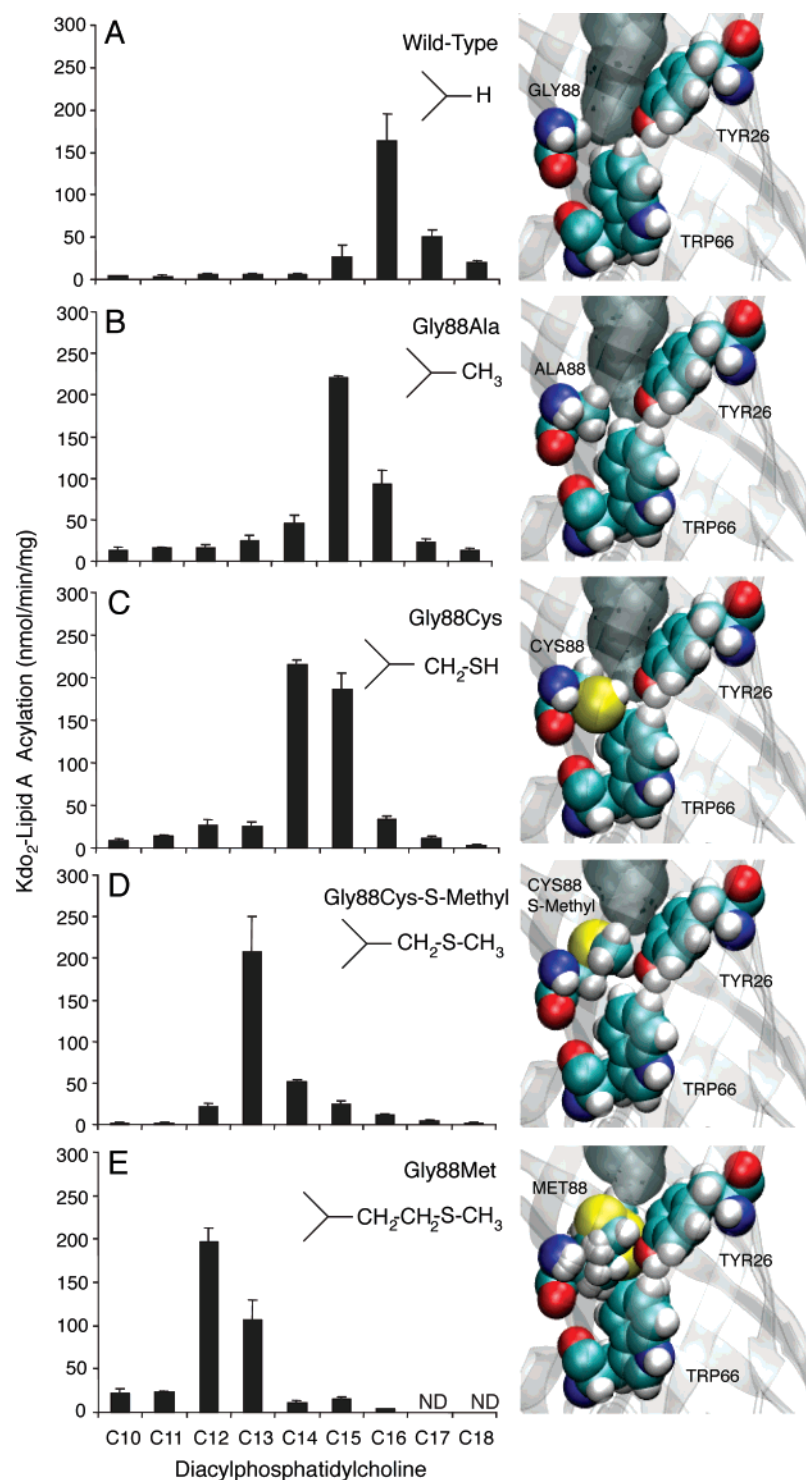
FIGURE 8: Hydrocarbon ruler analysis of refolded PagP variants. Synthetic diacylphosphatidylcholines with saturated acyl chains varying in single methylene increments from 10 to 18 carbon atoms were used as donors for the enzymatic acylation of Kdo_2-lipid A. Panels A−E present acyl-chain selection profiles for the refolded PagP variants. The structure of PagP (PDB entry 1THQ) emphasizing the positions of Gly88 and the exciton interaction between Tyr26 and Trp66 is shown at the right of panel A. Contouring reveals the β-barrel interior region after removal of the LDAO detergent molecule. In silico mutagenesis followed by simulated annealing was performed to reveal a predicted orientation of the PagP Gly88 substitutions, which are shown at the right of panels B−E. ND means not detected.

was not demonstrated until much later (*19*). Exciton coupling between Trp47 and Trp74 in *E. coli* dihydrofolate reductase was identified as the source of the first transient that can be detected by stopped flow in the refolding of the urea-denatured enzyme (*50*). More recently, a Gly95Ala mutation has been shown to abolish the Trp−Trp exciton, whereas binding of methotrexate restores it (*51*). Given the forecasted output of current structural proteomics consortia, it is likely

that the pool of proteins exhibiting clearly discernible exciton couplets will continue to grow rapidly into the future. Such knowledge will provide investigators with highly sensitive probes for monitoring the functional effects of locally introduced structural alterations.

A case in point is revealed by our current study of PagP, which has a number of favorable features that made the study possible. (1) The compact β-barrel structure of PagP produces

a relatively weak backbone CD that makes obvious the overlapping exciton couplet. (2) PagP can resolve methylene units in the acyl chains of its lipid substrate by using a molecular measuring device known as a hydrocarbon ruler, the floor of which is located in the proximity of the interacting exciton partners. (3) PagP is an extremely stable small protein that can be unfolded and refolded in vitro, enabling the transient exposure of buried functional groups for chemical modification. The fact that PagP is an integral membrane protein makes these favorable features all the more remarkable. Consequently, PagP beautifully demonstrates both the sensitivity of the exciton and how it can be employed as a spectroscopic probe to monitor a local structural perturbation.

The PagP hydrocarbon ruler was identified in a prior X-ray structure determination (*11*) and validated in that study by using enzyme that had been purified directly from membranes (*21*). However, the LDAO detergent used to purify the enzyme is a competitive inhibitor (*11*) and must be exchanged by dilution of the enzyme into a reaction cocktail that includes *n*-dodecyl β-D-maltoside or another detergent that supports PagP activity (*21*). While PagP purified directly from membranes is obtained at ~1 mg/mL (*21*), PagP can also be expressed without its N-terminal signal peptide, purified in an unfolded state, and reliably refolded in LDAO to reach a concentration of >10 mg/mL (*10*, *11*). Consequently, LDAO can be removed more effectively by dilution when using refolded PagP, which gives more reliable results in the enzyme assays. By using refolded PagP derivatives in this investigation, we observed for the first time that Gly88 substitutions, with the exception of the Cys mutation, modulate hydrocarbon ruler acyl-chain selection with methylene unit precision.

The predicted interactions of the Cys sulfhydryl group with the Trp66 and Tyr26 aromatic side chains can explain our main experimental observations that Gly88Cys PagP is both devoid of the exciton and compromised in terms of acyl-chain selection. Our simulated annealing experiments demonstrate that the amino acid substitutions observed experimentally to retain the exciton are advancing upward into the hydrocarbon ruler floor, while the one side chain that is able to recede downward (Cys) is observed to extinguish the exciton. The question of why the Cys sulfhydryl group would prefer the position between Tyr26 and Trp66 instead of inside the hydrophobic hydrocarbon ruler pocket remains. The hydrocarbon ruler floor in PagP marks the boundary between the upper hydrophobic and lower polar interior regions of the β-barrel (*11*), which might indicate that the Cys sulfhydryl group has an inherent tendency to seek out a more polar microenvironment. Hydrophobicity scales derived primarily from α-helical transmembrane domains typically identify Cys as being hydrophobic (*52*), but Cys in an α-helix normally donates a hydrogen bond to the carbonyl oxygen atom of the preceding peptide bond (*53*). In contrast, the sulfhydryl group of Gly88Cys PagP is forced into a β-structured conformation where it is faced above with nonpolar and below with polar environments. In the absence of a suitable hydrogen bond acceptor, the Cys sulfhydryl group appears to have rotated about its χ_1 dihedral angle to establish a weak electrostatic interaction with the Tyr26 hydroxyl group and/ or a so-called π (aromatic)−lone pair (sulfur) attraction with Trp66 (*54*). The polarizability of the sulfur atom and the

acidity of the sulfhydryl group are reported to promote its interaction with aromatic partners (*55*). Although our force field contains only partial point charges on each nucleus, which is but a rough approximation to the electronic distribution associated with (pure and hybrid) p orbitals, the force field may be capable of capturing these effects qualitatively.

The lactose permease provides an example of an α-helical transmembrane protein in which substitutions of Cys for Gly have had unpredictable effects on protein stability. The replacement of Cys154 with Gly within a transmembrane domain of the lactose permease has been shown to have stabilizing effects that are incompatible with active transport but necessary to obtain crystals for determining the structure by X-ray diffraction (*56*, *57*). Only Cys at position 154 was capable of introducing a local instability that was necessary for normal transport (*58*). The lactose permease in this region includes local distortions of helical conformation and close packing interactions with several aromatic partners. Perhaps the unusual physical properties associated with Cys154 in lactose permease have in common with Gly88Cys PagP the need to establish interactions with aromatic side chains. Clearly, the PagP hydrocarbon ruler affords unique opportunities to evaluate the physical forces at work in determining membrane protein stability. Our ability to enzymatically synthesize endotoxin analogues with defined acyl-chain substitutions might also reveal pharmacologically interesting derivatives, because acyl-chain length is known to be an important factor in determining endotoxin structure− activity relationships (*59*).

ACKNOWLEDGMENT

SUPPORTING INFORMATION AVAILABLE

Oligonucleotide primers used for site-directed mutagenesis and cloning (Table S1), far-UV CD spectra of PagP at different temperatures (Figure S1), analysis of PagP Trp66 mutants folded in vivo (Figure S2), and theoretical CD spectra of PagP, its in silico aromatic amino acid substitutions, and their difference spectra (Figure S3). This material is available free of charge via the Internet at http:// pubs.acs.org.

REFERENCES

1. Vance, D. E., and Vance, J. E. (2002) *Biochemistry of Lipids, Lipoproteins, and Membranes*, Elsevier, Amsterdam.
2. Dowhan, W. (1997) Molecular basis for membrane phospholipid diversity: Why are there so many lipids? *Annu. Rev. Biochem. 66*, 199−232.
3. Zhang, Y. M., White, S. W., and Rock, C. O. (2006) Inhibiting bacterial fatty acid synthesis, *J. Biol. Chem. 281*, 17541−17544.
4. Bracey, M. H., Cravatt, B. F., and Stevens, R. C. (2004) Structural commonalities among integral membrane enzymes, *FEBS Lett. 567*, 159−165.

5. Long, S. B., Casey, P. J., and Beese, L. S. (1998) Cocrystal structure of protein farnesyltransferase complexed with a farnesyl diphosphate substrate, *Biochemistry 37*, 9612−9618.

6. Wyckoff, T. J., Lin, S., Cotter, R. J., Dotson, G. D., and Raetz, C. R. (1998) Hydrocarbon rulers in UDP-*N*-acetylglucosamine acyltransferases, *J. Biol. Chem. 273*, 32369−32372.

7. White, S. H., Ladokhin, A. S., Jayasinghe, S., and Hristova, K. (2001) How membranes shape protein structure, *J. Biol. Chem. 276*, 32395−32398.

8. Snijder, H. J., Ubarretxena-Belandia, I., Blaauw, M., Kalk, K. H., Verheij, H. M., Egmond, M. R., Dekker, N., and Dijkstra, B. W. (1999) Structural evidence for dimerization-regulated activation of an integral membrane phospholipase, *Nature 401*, 717−721.

9. Rutten, L., Geurtsen, J., Lambert, W., Smolenaers, J. J., Bonvin, A. M., de Haan, A., van der Ley, P., Egmond, M. R., Gros, P., and Tommassen, J. (2006) Crystal structure and catalytic mechanism of the LPS 3-*O*-deacylase PagL from *Pseudomonas aeruginosa*, *Proc. Natl. Acad. Sci. U.S.A. 103*, 7071−7076.

10. Hwang, P. M., Choy, W. Y., Lo, E. I., Chen, L., Forman-Kay, J. D., Raetz, C. R., Prive, G. G., Bishop, R. E., and Kay, L. E. (2002) Solution structure and dynamics of the outer membrane enzyme PagP by NMR, *Proc. Natl. Acad. Sci. U.S.A. 99*, 13560−13565.

11. Ahn, V. E., Lo, E. I., Engel, C. K., Chen, L., Hwang, P. M., Kay, L. E., Bishop, R. E., and Prive, G. G. (2004) A hydrocarbon ruler measures palmitate in the enzymatic acylation of endotoxin, *EMBO J. 23*, 2931−2941.

12. Harada, N., and Nakanishi, K. (1983) *Circular dichroic spectroscopy: Exciton coupling in organic stereochemistry*, University Science Books, Mill Valley, CA.

13. Schellman, J. A. (1968) Symmetry rules for optical rotation, *Acc. Chem. Res. 1*, 144−151.

14. Davydov, A. S. (1971) *Theory of molecular excitons. Translated from Russian by Stephen B. Dresner*, New American ed., Plenum Press, New York.

15. Woody, R. W. (1995) Circular dichroism, *Methods Enzymol. 246*, 34−71.

16. Woody, R. W. (1994) Contributions of tryptophan side chains to the far-ultraviolet circular dichroism of proteins, *Eur. Biophys. J. 23*, 253−262.

17. Sreerama, N., and Woody, R. W. (2004) On the analysis of membrane protein circular dichroism spectra, *Protein Sci. 13*, 100−112.

18. Sreerama, N., and Woody, R. W. (2004) Computation and analysis of protein circular dichroism spectra, *Methods Enzymol. 383*, 318−351.

19. Grishina, I. B., and Woody, R. W. (1994) Contributions of tryptophan side chains to the circular dichroism of globular proteins: Exciton couplets and coupled oscillators, *Faraday Discuss.*, 245−262.

20. Bishop, R. E. (2005) The lipid A palmitoyltransferase PagP: Molecular mechanisms and role in bacterial pathogenesis, *Mol. Microbiol. 57*, 900−912.

21. Bishop, R. E., Gibbons, H. S., Guina, T., Trent, M. S., Miller, S. I., and Raetz, C. R. (2000) Transfer of palmitate from phospholipids to lipid A in outer membranes of Gram-negative bacteria, *EMBO J. 19*, 5071−5080.

22. Kamio, Y., and Nikaido, H. (1976) Outer membrane of *Salmonella typhimurium*: Accessibility of phospholipid head groups to phospholipase c and cyanogen bromide activated dextran in the external medium, *Biochemistry 15*, 2561−2570.

23. Nikaido, H. (2003) Molecular basis of bacterial outer membrane permeability revisited, *Microbiol. Mol. Biol. Rev. 67*, 593−656.

24. Guo, L., Lim, K. B., Poduje, C. M., Daniel, M., Gunn, J. S., Hackett, M., and Miller, S. I. (1998) Lipid A acylation and bacterial resistance against vertebrate antimicrobial peptides, *Cell 95*, 189−198.

25. Kawasaki, K., Ernst, R. K., and Miller, S. I. (2004) 3-*O*-Deacylation of lipid A by PagL, a PhoP/PhoQ-regulated deacylase of *Salmonella typhimurium*, modulates signaling through toll-like receptor 4, *J. Biol. Chem. 279*, 20044−20048.

26. Hwang, P. M., Bishop, R. E., and Kay, L. E. (2004) The integral membrane enzyme PagP alternates between two dynamically distinct states, *Proc. Natl. Acad. Sci. U.S.A. 101*, 9618−9623.

27. Jia, W., Zoeiby, A. E., Petruzziello, T. N., Jayabalasingham, B., Seyedirashti, S., and Bishop, R. E. (2004) Lipid trafficking controls endotoxin acylation in outer membranes of *Escherichia coli*, *J. Biol. Chem. 279*, 44966−44975.

28. Gill, S. C., and von Hippel, P. H. (1989) Calculation of protein extinction coefficients from amino acid sequence data, *Anal. Biochem. 182*, 319−326.

29. Heinrikson, R. L. (1971) The selective *S*-methylation of sulfhydryl groups in proteins and peptides with methyl-*p*-nitrobenzenesulfonate, *J. Biol. Chem. 246*, 4090−4096.

30. Whitelegge, J. P., le Coutre, J., Lee, J. C., Engel, C. K., Prive, G. G., Faull, K. F., and Kaback, H. R. (1999) Toward the bilayer proteome, electrospray ionization-mass spectrometry of large, intact transmembrane proteins, *Proc. Natl. Acad. Sci. U.S.A. 96*, 10695−10698.

31. Smith, P. K., Krohn, R. I., Hermanson, G. T., Mallia, A. K., Gartner, F. H., Provenzano, M. D., Fujimoto, E. K., Goeke, N. M., Olson, B. J., and Klenk, D. C. (1985) Measurement of protein using bicinchoninic acid, *Anal. Biochem. 150*, 76−85.

32. Edelhoch, H. (1967) Spectroscopic determination of tryptophan and tyrosine in proteins, *Biochemistry 6*, 1948−1954.

33. Pace, C. N., Vajdos, F., Fee, L., Grimsley, G., and Gray, T. (1995) How to measure and predict the molar absorption coefficient of a protein, *Protein Sci. 4*, 2411−2423.

34. Woody, R. W., and Sreerama, N. (1999) Comment on 'Improving protein circular dichroism calculations in the far-ultraviolet through reparameterizing the amide chromophore' [*J. Chem. Phys. 109*, 782 (1998)], *J. Chem. Phys. 111*, 2844−2845.

35. Kanipes, M. I., Lin, S., Cotter, R. J., and Raetz, C. R. (2001) Ca^{2+}-induced phosphoethanolamine transfer to the outer 3-deoxy-D-*manno*-octulosonic acid moiety of *Escherichia coli* lipopolysaccharide. A novel membrane enzyme dependent upon phosphatidylethanolamine, *J. Biol. Chem. 276*, 1156−1163.

36. Lee, C. H., and Tsai, C. M. (1999) Quantification of bacterial lipopolysaccharides by the purpald assay: Measuring formaldehyde generated from 2-keto-3-deoxyoctonate and heptose at the inner core by periodate oxidation, *Anal. Biochem. 267*, 161−168.

37. Feller, S. E., and MacKerell, A. D. (2000) An improved empirical potential energy function for molecular simulations of phospholipids, *J. Phys. Chem. B 104*, 7510−7515.

38. Jorgensen, W. L., Chandrasekhar, J., Madura, J. D., Impey, R. W., and Klein, M. L. (1983) Comparison of simple potential functions for simulating liquid water, *J. Chem. Phys. 79*, 926−935.

39. Brooks, B. R., Bruccoleri, R. E., Olafson, B. D., States, D. J., Swaminathan, S., and Karplus, M. (1983) Charmm: A Program for Macromolecular Energy, Minimization, and Dynamics Calculations, *J. Comput. Chem. 4*, 187−217.

40. MacKerell, A. D., Bashford, D., Bellott, M., Dunbrack, R. L., Evanseck, J. D., Field, M. J., Fischer, S., Gao, J., Guo, H., Ha, S., Joseph-McCarthy, D., Kuchnir, L., Kuczera, K., Lau, F. T. K., Mattos, C., Michnick, S., Ngo, T., Nguyen, D. T., Prodhom, B., Reiher, W. E., Roux, B., Schlenkrich, M., Smith, J. C., Stote, R., Straub, J., Watanabe, M., Wiorkiewicz-Kuczera, J., Yin, D., and Karplus, M. (1998) All-atom empirical potential for molecular modeling and dynamics studies of proteins, *J. Phys. Chem. B 102*, 3586−3616.

41. Humphrey, W., Dalke, A., and Schulten, K. (1996) VMD: Visual molecular dynamics, *J. Mol. Graphics 14*, 33−38, 27−28.

42. Smart, O. S., Goodfellow, J. M., and Wallace, B. A. (1993) The pore dimensions of gramicidin A, *Biophys. J. 65*, 2455−2460.

43. DeLano, W. L. (2002) *The PyMOL Molecular Graphics System*, DeLano Scientific, San Carlos, CA.

44. Saxena, V. P., and Wetlaufer, D. B. (1971) A new basis for interpreting the circular dichroic spectra of proteins, *Proc. Natl. Acad. Sci. U.S.A. 68*, 969−972.

45. Mogensen, J. E., and Otzen, D. E. (2005) Interactions between folding factors and bacterial outer membrane proteins, *Mol. Microbiol. 57*, 326−346.

46. Gellman, S. H. (1991) On the role of methionine residues in the sequence-independent recognition of nonpolar protein surfaces, *Biochemistry 30*, 6633−6636.

47. Gasymov, O. K., Abduragimov, A. R., Yusifov, T. N., and Glasgow, B. J. (2002) RET and anisotropy measurements establish the proximity of the conserved Trp17 to Ile98 and Phe99 of tear lipocalin, *Biochemistry 41*, 8837−8848.

48. Nakao, M., Maki, K., Arai, M., Koshiba, T., Nitta, K., and Kuwajima, K. (2005) Characterization of kinetic folding intermediates of recombinant canine milk lysozyme by stopped-flow circular dichroism, *Biochemistry 44*, 6685−6692.

49. McConn, J., Fasman, G. D., and Hess, G. P. (1969) Conformation of the high pH form of chymotrypsin, *J. Mol. Biol. 39*, 551–562.

50. Kuwajima, K., Garvey, E. P., Finn, B. E., Matthews, C. R., and Sugai, S. (1991) Transient intermediates in the folding of dihydrofolate reductase as detected by far-ultraviolet circular dichroism spectroscopy, *Biochemistry 30*, 7693–7703.

51. Svensson, A. K., O'Neill, J. C., Jr., and Matthews, C. R. (2003) The coordination of the isomerization of a conserved non-prolyl cis peptide bond with the rate-limiting steps in the folding of dihydrofolate reductase, *J. Mol. Biol. 326*, 569–583.

52. Bowie, J. U. (2005) Solving the membrane protein folding problem, *Nature 438*, 581–589.

53. Gray, T. M., and Matthews, B. W. (1984) Intrahelical hydrogen bonding of serine, threonine and cysteine residues within α-helices and its relevance to membrane-bound proteins, *J. Mol. Biol. 175*, 75–81.

54. Duan, G., Smith, V. H., Jr., and Weaver, D. F. (2001) Characterization of aromatic-thiol π-type hydrogen bonding and phenylalanine-cysteine side chain interactions through *ab initio* calculations and protein database analyses, *Mol. Phys. 99*, 1689–1699.

55. Meyer, E. A., Castellano, R. K., and Diederich, F. (2003) Interactions with aromatic rings in chemical and biological recognition, *Angew. Chem., Int. Ed. 42*, 1210–1250.

56. Smirnova, I. N., and Kaback, H. R. (2003) A mutation in the lactose permease of *Escherichia coli* that decreases conformational flexibility and increases protein stability, *Biochemistry 42*, 3025–3031.

57. Abramson, J., Smirnova, I., Kasho, V., Verner, G., Kaback, H. R., and Iwata, S. (2003) Structure and mechanism of the lactose permease of *Escherichia coli*, *Science 301*, 610–615.

58. Ermolova, N. V., Smirnova, I. N., Kasho, V. N., and Kaback, H. R. (2005) Interhelical packing modulates conformational flexibility in the lactose permease of *Escherichia coli*, *Biochemistry 44*, 7669–7677.

59. Stover, A. G., Da Silva Correia, J., Evans, J. T., Cluff, C. W., Elliott, M. W., Jeffery, E. W., Johnson, D. A., Lacy, M. J., Baldridge, J. R., Probst, P., Ulevitch, R. J., Persing, D. H., and Hershberg, R. M. (2004) Structure–activity relationship of synthetic toll-like receptor 4 agonists, *J. Biol. Chem. 279*, 4440–4449.

SUPPORTING INFORMATION:

*Gauging a Hydrocarbon Ruler by an Intrinsic Exciton Probe*

M. Adil Khan, Chris Neale, Catherine Michaux, Régis Pomès, Gilbert G. Privé, Robert W. Woody, and Russell E. Bishop

Table S1: Oligonucleotide primers used for site-directed mutagenesis and cloning[1]

|	
G88A.top	5'-CCGATTGCCGGATAC<u>GCT</u>TGGGAAAGTACCTG-3'
G88A.bot	5'-CAGGTACTTTCCCA<u>AGC</u>GTATCCGGCAATCGG-3'
G88C.top	5'-CCGATTGCCGGATAC<u>TGC</u>TGGGAAAGTACCTG-3'
G88C.bot	5'-CAGGTACTTTCCCA<u>GCA</u>GTATCCGGCAATCGG-3'
G88M.top	5'-CCGATTGCCGGATAC<u>ATG</u>TGGGAAAGTACCTGG-3'
G88M.bot	5'-CCAGGTACTTTCCCA<u>CAT</u>GTATCCGGCAATCGG-3'
W66H.top	5'-GAAAAAGGAAAC<u>CAC</u>CATGGCCTGTATGCCATGGC-3'
W66H.bot	5'-GCCATGGCATACAGGCCATG<u>GTG</u>GTTTCCTTTTTC-3'
W66F.top	5'-GAAAAAGGAAAC<u>TTC</u>CATGGCCTGTATGCCATGGC-3'
W66F.bot	5'-GCCATGGCATACAGGCCATG<u>GAA</u>GTTTCCTTTTTC-3'
Y26F.top[2]	5'-GGAACATTATGATTTA<u>TTC</u>ATTCCTGCCATCACCTGG-3'
Y26F.bot[2]	5'-CCAGGTGATGGCAGGAAT<u>GAA</u>TAAATCATAATGTTCC-3'
Forward	5'-GGTAAAGCATATGAACGCAGATGAGTGGAT-3'
Reverse	5'-GCTCAGCGGTGGCAGCAG-3'

[1] Mutagenized codons are underlined.

[2] The Y26F mutation was generated in pETCrcAHΔS for direct expression without the *N*-terminal signal peptide. The remaining mutations were generated first in pETCrcAH with the intact signal peptide, and then amplified by PCR using the primers Forward and Reverse; subcloning into pETCrcAHΔS by *Nde*I/*Xho*I digestion and ligation was then verified by double strand sequencing.
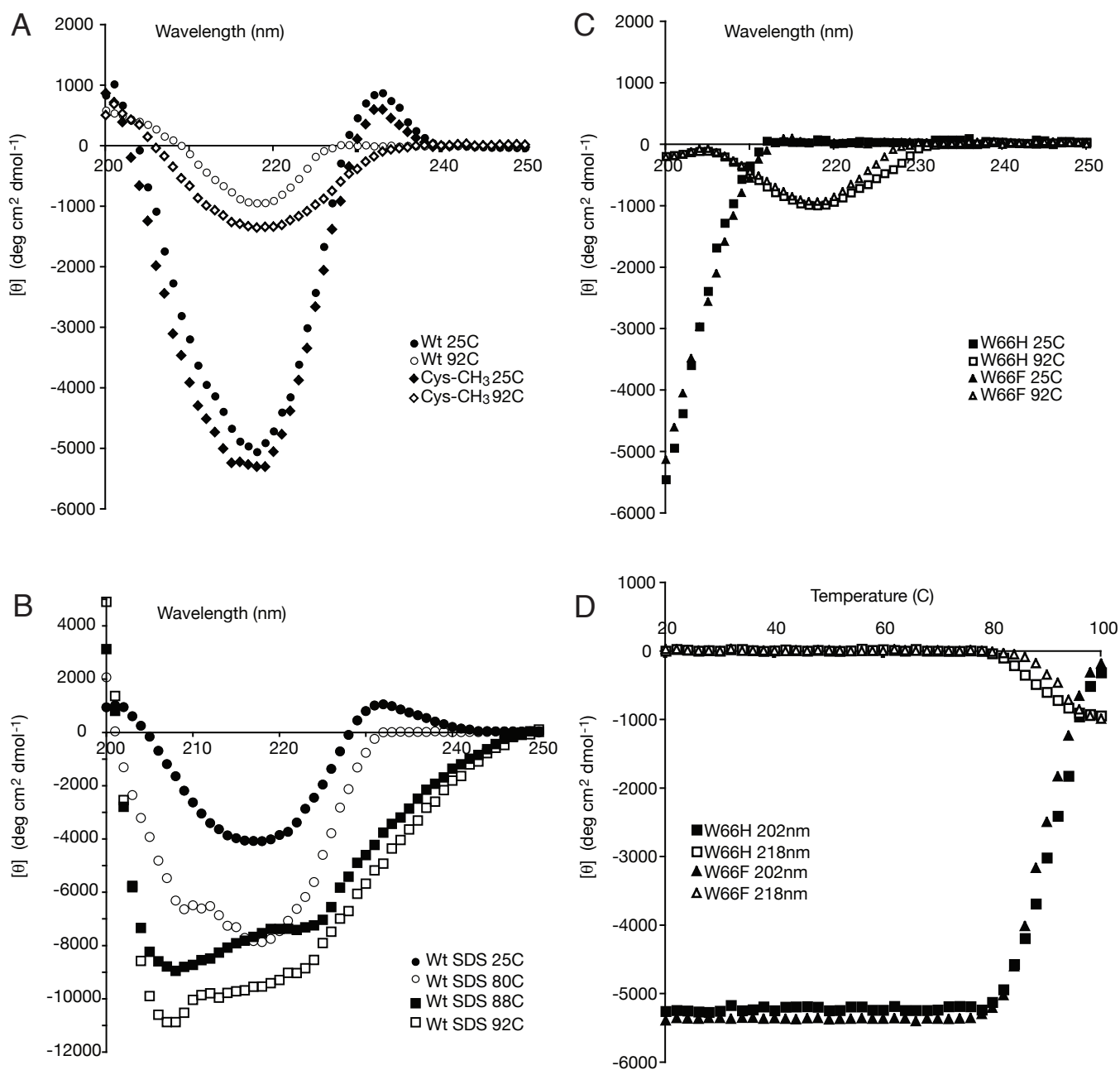
Figure S1. Far-UV CD spectra of PagP at different temperatures. Spectra were taken at the indicated temperatures after a 15 minute equilibration using PagP derivatives that were refolded in LDAO as indicated in Experimental Procedures. Panel A shows spectra for wild-type (Wt) and G88C-*S*-methyl PagP. Panel B shows spectra for Wt PagP refolded in LDAO and diluted into 1% SDS. Panel C shows W66H and W66F PagP, whereas Panel D shows their thermal precipitation curves.
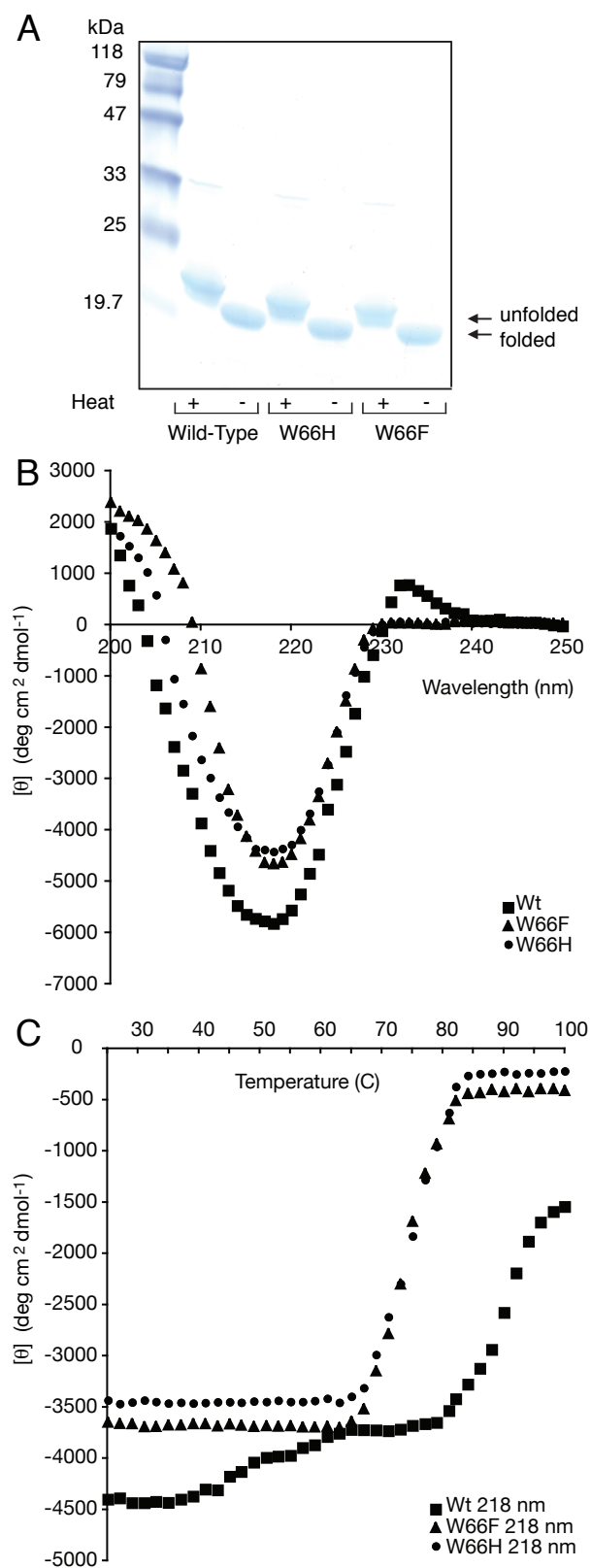
Figure S2. Analysis of PagP W66 mutants folded *in vivo*. Wild-type (Wt) is compared with W66H and W66F PagP mutants. Panel A shows SDS-PAGE, Panel B shows far-UV CD, and Panel C shows thermal precipitation curves following the loss of ellipticity at 218 nm.
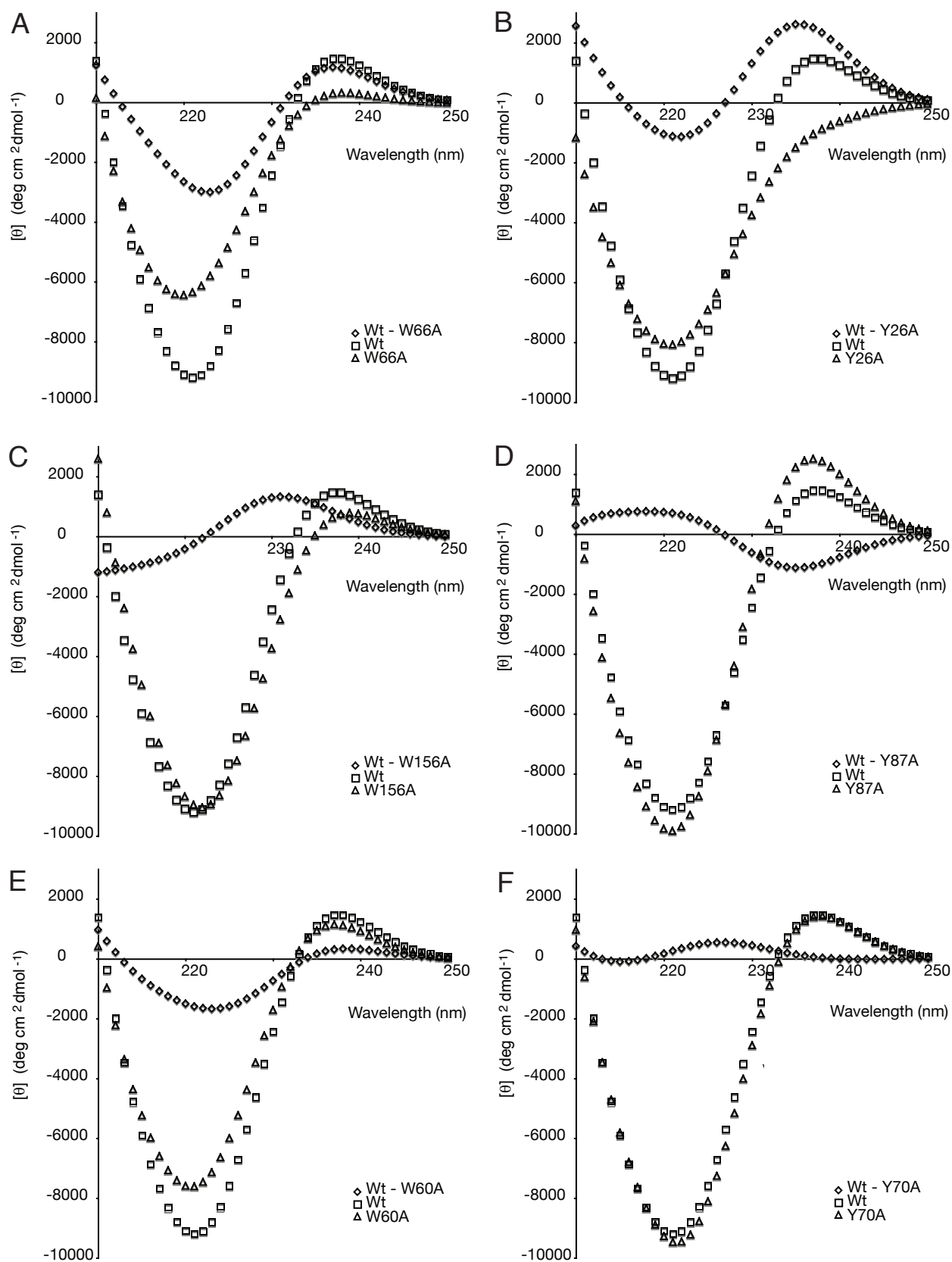
Figure S3. Theoretical CD spectra of PagP, its *in silico* aromatic amino acid substitutions, and their difference spectra. Wild-type (Wt) is compared with W66A, Y26A, W156A, Y87A, W60A, and Y70A PagP in panels A - F, respectively.